Winter JJ, Anderson M, Blades K, Brassington C, Breeze AL, Chresta C, Embrey K, Fairley G, Faulder P, Finlay MR, Kettle JG, Nowak T, Overman R, Patel SJ, Perkins P, Spadola L, Tart J, Tucker JA, Wrigley G.

Small Molecule Binding Sites on the Ras:SOS Complex Can Be Exploited for Inhibition of Ras Activation.

***Journal of Medicinal Chemistry* 2015, 58(5), 2265-2274.**

Small molecule binding sites on the Ras:SOS complex can be exploited for inhibition of Ras activation

Jon J. G. Winter,[a,*] Malcolm Anderson,[a,b] Kevin Blades,[a] Claire Brassington,[a] Alexander L. Breeze,[a,c] Christine Chresta,[a] Kevin Embrey,[a] Gary Fairley,[a] Paul Faulder,[a,d] M. Raymond V. Finlay,[a] Jason G. Kettle,[a] Thorsten Nowak,[a,e] Ross Overman,[a] S. Joe Patel,[a,f] Paula Perkins,[a,g] Loredana Spadola,[a] Jonathan Tart,[a] Julie A. Tucker[a,h] & Gail Wrigley[a]

[a] AstraZeneca, Alderley Park, Macclesfield, Cheshire, SK10 4TG, United Kingdom. * Author to whom correspondence should be addressed (email: jon.winter@astrazeneca.com). *Present Author Addresses*: [b] Waters Corporation, Atlas Park, Simonsway, Manchester, M22 5PP, United Kingdom (M.A.); [c] Astbury Centre for Structural Molecular Biology, University of Leeds, Leeds, LS2 9JT, United Kingdom (A.L.B.); [d] Elixir Software Ltd., Lynwood House, Rowton Lane, Rowton, Chester, Cheshire, CH3 6AT, United Kingdom (P.F.); [e] C4X Discovery Ltd., Unit 310 Ducie House, Ducie Street, Manchester, M1 2JW, United Kingdom (T.N.); [f] AstraZeneca, Gatehouse Park, 35 Gatehouse Drive, Waltham, MA 02451, USA (S.J.P.); [g] 45 Sycamore Crescent, Macclesfield, Cheshire, SK11 8LW, United Kingdom (P.P.); [h] Northern Institute for Cancer Research, Paul O'Gorman Building, Newcastle University, Framlington Place, Newcastle upon Tyne, NE2 4HH, United Kingdom (J.A.T.).

ABSTRACT

Constitutively active mutant KRas displays a reduced rate of GTP hydrolysis via both intrinsic and GTPase-activating protein-catalysed mechanisms, resulting in the perpetual activation of Ras pathways. We describe a fragment screening campaign using X-ray crystallography that led to the discovery of three fragment binding sites on the Ras:SOS complex. The identification of tool compounds binding at each of these sites allowed exploration of two new approaches to Ras pathway inhibition by stabilising or covalently modifying the Ras:SOS complex to prevent the reloading of Ras with GTP. Initially, we identified ligands that bound reversibly to the Ras:SOS complex in two distinct sites, but these compounds were not sufficiently potent inhibitors to validate our stabilisation hypothesis. We conclude by demonstrating that covalent modification of Cys118 on Ras leads to a novel mechanism of inhibition of the SOS-mediated interaction between Ras and Raf, and is effective at inhibiting the exchange of labelled GDP in both mutant (G12C and G12V) and wild type Ras.

INTRODUCTION

Members of the Ras family of small GTPases function as simple molecular switches. Ras is transformed into its active, GTP-bound state by interaction with a guanine nucleotide exchange factor (GEF) such as SOS, which catalyses release of GDP and allows binding of the more abundant GTP. In this active conformation, Ras is recognised by a range of direct effectors such as Raf, PI3 kinase and Ral proteins, which in turn can drive proliferation, survival and metastasis. Under normal physiological conditions, the intrinsic GTPase activity of Ras hydrolyses GTP back to GDP, causing inactivation. This process is significantly accelerated by GTPase activating proteins (GAPs) which can increase the intrinsic hydrolysis rate by up to 1000-fold. Mutations in the *KRAS* oncogene are present in a significant proportion of human tumors. Estimates of mutation prevalence vary by tumor type, however, they are known to be particularly associated with carcinomas of the lung, colon and pancreas.[1] Aberrant *KRAS* signaling drives an aggressive proliferative phenotype that is resistant to therapy and results in poor prognosis. These mutations, most commonly G12D and G12V, impair the ability of Ras to hydrolyse the terminal phosphate of GTP, limit sensitivity to GAP stimulation, and result in perpetual activation of Ras pathways.

Ras may be considered the archetypal 'intractable target' in oncology. Despite its characterisation over 30 years ago, reports on agents that directly target Ras, or indeed any GTPase, are limited.[2] Most drug discovery efforts have been directed against its more tractable downstream effectors, for example inhibitors of the kinases Raf and MEK.[3] Guanine nucleotides exhibit picomolar affinity for Ras; therefore competitive binding at the nucleoside site is unlikely to be feasible, in contrast to conventional ATP mimetics in the field of kinase inhibition. It is possible that binding to Ras in an allosteric manner may promote loss of nucleotide, and indeed such a mechanism has been speculated for a reported inhibitor of the related GTPase Rac1, although no structural evidence for this is available[4] and no obvious structural opportunities exist for Ras. A small molecule which is able to bind to Ras-GDP and block SOS binding should be able to limit Ras activation. This approach to Ras inhibition via disruption of a key protein-protein interaction has recently achieved validation by two independent groups. Sun *et al.* have reported a diverse array of small molecules that bind in a hydrophobic pocket located between the α2 helix of switch II (residues 60-74) and the central β sheet of KRas (G12D).[5] These were identified using an NMR-based screen of 11,000 fragments using ^{15}N-labelled protein, with the binding mode confirmed by co-crystallization.

Simultaneously, Maurer *et al.* reported structurally distinct small molecules that also bind to this pocket.[6] Again, an NMR screen of 3,300 fragments using full-length KRas4B (G12D) yielded hits whose structures in

complex with KRas were confirmed by X-ray crystallography. Both approaches have demonstrated that binding at this site in the affinity range of 100s of μM is sufficient to inhibit the SOS-mediated activation of KRas. Since oncogenic KRas is locked in its active GTP-bound state, it is unclear whether such a strategy that prevents activation might be efficacious in tumors harbouring mutations in KRas, although a role in those tumors with active signalling through wild type Ras is plausible. Recent publications by Ostrem *et al.* and Lim *et al.* has shown that inhibition of the GTPase activity of the KRas(G12C) mutant can be achieved by irreversible binding of cysteine-reactive small molecules. Compounds are described which react close to the nucleotide binding site at Cys12, and either allosterically control the GTP affinity of the mutant[7] or directly block the ability of GTP to bind.[8] The approach relies on this specific KRas mutation to introduce the reactive cysteine thiolate, resulting in compounds which, while selective over wild type Ras, cannot inhibit other Ras mutants and which may be susceptible to resistance.

An alternative approach to preventing Ras activation may be envisioned in which a small molecule is able to bind at the interface of the Ras:SOS complex. Conceptually, such an agent might be able to stabilise these partners, inhibiting dissociation of SOS, and so prevent reloading of Ras with GTP. In theory this avoids some of the challenges implicit in other approaches, such as nucleotide competition, requiring inhibition of larger protein-protein interfaces, or mutant specificity, and might offer a more tractable binding pocket than the relatively featureless Ras protein alone. Precedent for this approach emerges from the observation that the natural product Brefeldin A (BFA) binds to a related small GTPase, Arf, and its exchange factor, ARNO.[9] In this complex, GDP is also present, resulting in a quaternary complex where BFA is located in a hydrophobic pocket at the Arf-ARNO interface, one-third of which is contributed by ARNO and two-thirds by Arf. BFA acts as an uncompetitive inhibitor that stabilises an abortive Arf-GDP-ARNO complex resulting in inhibition of the secretory pathway in eukaryotic cells.[10]

Compounds have recently been reported by Burns *et al.* which bind to the Ras:SOS complex and increase the rate of SOS-mediated nucleotide exchange.[11] This is the reverse of the desired effect for an oncology therapy but it is notable that a small molecule can affect this pathway.

Although there is no reported structure of KRas in complex with an exchange factor, the structure of the closely homologous isoform HRas in 1:1 complex with a catalytic domain construct of SOS is known.[12] Inhibitors of activation of KRas were our primary goal owing to the greater frequency of oncogenic mutations in KRas than for other Ras isoforms, however, molecular modelling predicted high homology to HRas in complex with SOS, so this was utilized as a surrogate. Indeed, in the previously described KRas fragment screen, inhibitors were reported to

cross-react with both wild type K- and HRas.[5] We therefore sought to use the HRas:SOS binary complex to screen for potential ligands via X-ray crystallography, through a process of soaking 'cocktails' of small fragments into crystals of the complex. Such an approach has been reported in inhibitor design against the bacterial enzyme nucleoside 2-deoxyribosyltransferase.[13]

RESULTS

X-ray screening of a fragment library

To obtain a crystal system suitable for X-ray fragment screening, a novel co-expression construct was generated comprising a C-terminal truncated HRas (1-166) and the catalytic domain of SOS encompassing the Ras exchanger motif and cdc25 domain (564-1049). This heterodimeric protein complex was stable during purification and used to reproduce the structural system described by Boriack-Sjodin *et al.*, wherein SOS has HRas bound to its catalytic site,[12] while the allosteric Ras binding site described by Margarit *et al.* is unoccupied.[14]

A library of 1160 fragments was organized into four-compound cocktails using an in-house shape fingerprint tool to maximize the shape diversity of compounds in each cocktail.[15] Protein crystals were soaked in a stabilizing solution containing a final concentration of 5 mM of each fragment for 1 hour prior to being flash frozen and stored for data collection using a synchrotron radiation source. Datasets were processed, structures solved and initial refinement carried out using in-house software pipelines. Electron density maps were visually inspected to identify fragment binding. We observed significant attrition where a large number of compound cocktails were observed to abolish diffraction from the soaked HRas:SOS crystals. Of the crystals that survived, 25% were found to have small molecules present at one or more binding sites on SOS and, more intriguingly, at the interface between HRas and SOS. We were able to determine binding affinities for the fragments identified by crystal soaking using TROSY-HSQC solution NMR titrations with stable isotope-labeled HRas:SOS complex. A full description of the experimental methods used can be found in the Supplementary Results section. Crystallographic data collection and refinement statistics are detailed in **Supplementary Table 1**.

This paper describes three distinct small molecule binding sites that were identified on the complex, summarized in **Figure 1**.

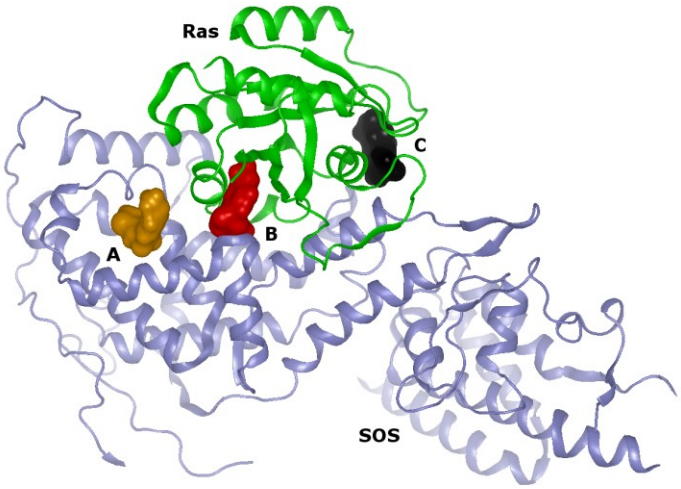

Figure 1 | Three fragment binding sites on the HRas:SOS complex. HRas in green, SOS in lilac. Fragment binding site A (gold) is located on SOS. Site B (red) is at the HRas:SOS binding interface. On the opposite face of the complex, covalent binding site C (black) is found on HRas.

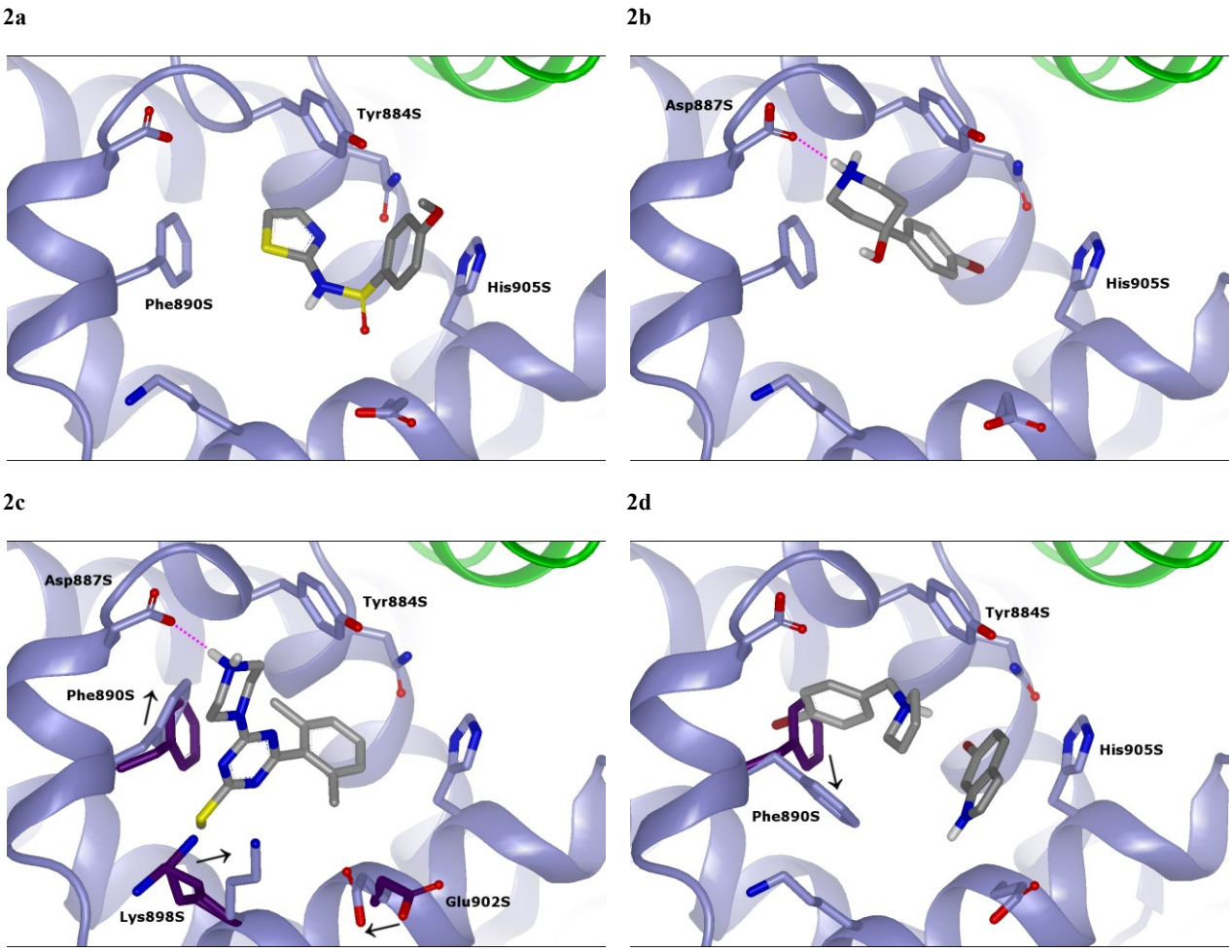

Figure 2 | Fragments binding at HRas:SOS site A. HRas colored green, SOS in lilac. Where side chain movements occur on ligand binding, their original positions in the HRas:SOS unbound structure *1BKD* are shown in dark purple for comparison, with arrows indicating direction of movement. (**a**) Binding of **1** results in no significant side chain movements. (**b**) The binding of **2** also causes no significant side chain perturbation. (**c**) Upon binding of **3**, side chain reorganization occurs at the front of the pocket opening a channel to accommodate the methylsulfanyl. (**d**) Simultaneous binding of **4a** and **4b** is accompanied by movement of Phe890S, opening up the back of the pocket.

Fragment binding site A on SOS

The fragment binding site we identified on the SOS protein (site A in **Fig. 1**) is a flexible bowl-shaped pocket lined with several residues showing mobile side chains. Upon binding of **1** to the SOS site A (**Fig. 2a**), no significant side-chain movements are observed relative to the unbound HRas:SOS structure (PDB *1BKD*). Binding appears to be

driven by aromatic ring interactions such as the edge-face interactions of the ligand thiazole with the phenyl ring of Phe890 of SOS ('Phe890S')[16] (~3.6 Å), and a π-stacking conformation between His905S (~3.8 Å) and the ligand phenyl ring.

Binding of **2** in site A occurs without significant perturbation of protein side chains (**Fig. 2b**). The key interaction is a hydrogen bond between the piperidine nitrogen and Asp887S (2.8 Å). The bromine atom of **2** is situated in a lipophilic pocket near His905S.

Binding of **3** at site A appears to be 'shape-driven' (**Fig. 2c**). An edge-face interaction is observed between Tyr884S and the ligand phenyl (~4 Å), and a π-stacking interaction between Phe890S and the triazine (~3.7 Å). Phe890S is displaced by ~1.8 Å and rotated compared with the unbound structure *1BKD*. The basic nitrogen of the ligand piperidine forms a hydrogen bond with the carboxylic acid of Asp887S (3.0 Å). Lys898S changes from a dual to a single occupancy state, moving 4.3 Å to avoid a steric clash with the methylsulfanyl group of **3**, with concomitant movement of Glu902S which forms a salt bridge with Lys898S (4.0 Å).

The crystal structure solved for **4a** and **4b** is notable because it comprises two fragments from the same cocktail which each bind to site A only in the presence of their partner (**Fig. 2d**). An NMR-derived pK_D was measurable for each fragment independently, however, given the small number of shifts observed, especially for **4b**, the binding sites monitored in the solution NMR experiments may not exactly coincide with that of the partnered binding observed in the crystal structure. In this structure Phe890S rotates 6.3 Å out towards solvent opening up a lipophilic pocket at the back of site A which is filled by the **4a** bromine. **4b** is stacked between His905S and the pyrrolidine of **4a**, whilst **4a** is sandwiched between Phe890S and Tyr884S, and lies perpendicular to the plane of **4b**.

Binding site A corresponds to the site recently reported by Burns, *et al*.[11] The three X-ray crystal structures they describe (*4NYI*, *4NYJ*, *4NYM*) show minimal side chain movements in site A compared with the unbound structure of SOS, and correspond most closely with our structures of **1** and **2** in complex with HRas:SOS (**Figs. 2a** & **2b**).

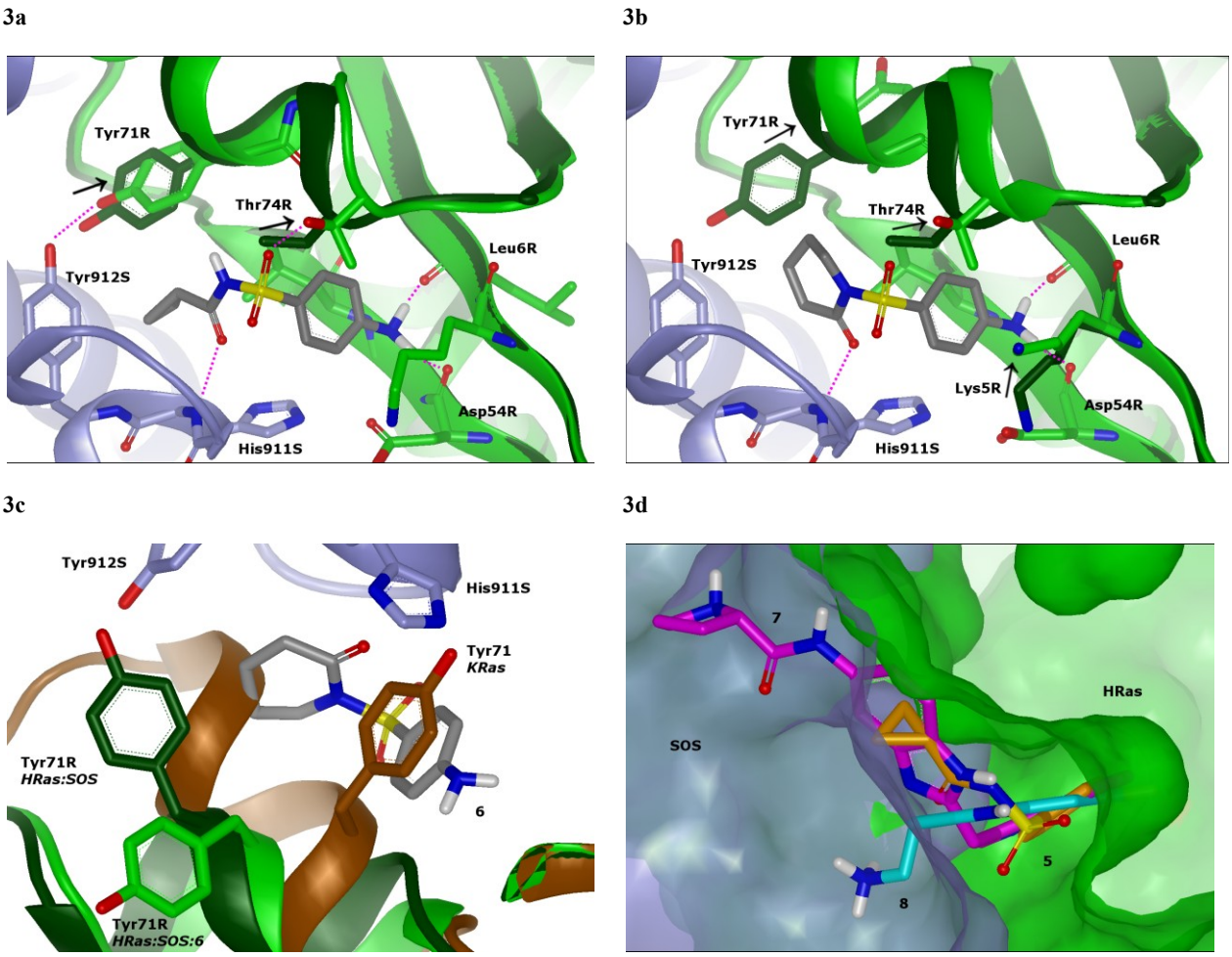

Figure 3 | Fragments binding at HRas:SOS site B. HRas colored green, SOS in lilac. Where side chain movements occur on ligand binding, their original positions in the HRas:SOS unliganded structure are shown in dark green for comparison. (**a**) **5** binds in site B at the interface between HRas and SOS, with resultant movements in HRas protein side chains shown. (**b**) **6** binding at the same location causes a larger shift in Tyr71R opening up a new pocket. (**c**) The Tyr71R side chain shows a wide range of conformations, as illustrated by an overlay of the KRas unbound structure *4EPR* (brown), HRas:SOS unliganded structure (dark green) and HRas:SOS:**6** complex structure (light green). (**d**) **5** (orange carbon atoms) binds in site B between the HRas (green) and SOS (lilac) surfaces in the HRas:SOS complex. In comparison, the KRas ligands **7**[5] (magenta) and **8**[6] (cyan) bind to KRas site 2 and place side chains into the space SOS would occupy in the HRas:SOS complex.

Fragment binding site B at the HRas:SOS interface

The binding site identified at the interface of HRas and SOS ('site B') corresponds to a site previously described in studies of uncomplexed Ras protein[5,6] ('site 2'). However, while Ras ligands **7** and **8**, which were identified in these studies, inhibit SOS-mediated nucleotide exchange by preventing the binding of SOS to Ras, the fragments **5** and **6** we identified as binding to site B interact with both Ras and SOS, and we hoped to show that this additional binding interaction may serve to stabilise the protein-protein interaction.

Fig. 3a shows **5** in complex with HRas:SOS occupying the largely solvent-inaccessible site B at the HRas:SOS interface. Hydrogen bonding interactions are observed between the aniline of **5** and the backbone carbonyls of Leu6R (3.2 Å) and Asp54R (3.0 Å). The carbonyl of the acylsulfonamide group forms an H-bond with the backbone NH of His911S (2.8 Å). An edge-face interaction between the phenyl ring of **5** and His911S is also observed (~3.5 Å). The hydroxyl group of Thr74R is positioned within H-bonding distance (2.8 Å) of one of the S=O bonds of the acylsulfonamide. The cyclopropyl ring is positioned between to Leu56R (~3.4 Å) and Tyr912S (~3.2 Å). A hydrogen-bonded tyrosine bridge (3.2 Å) between the two phenols of Tyr912S and Tyr71R links HRas and SOS. Comparison of the unbound structure (dark green) with this ligand-bound Ras:SOS complex shows limited movement for the majority of protein side chains in this region, with some notable exceptions. Thr74R moves 2.4 Å, making room for the ligand phenylsulfonamide. A small movement in the associated α-helix (residues Gln70R-Thr74R), opens up the binding pocket slightly. Tyr71R is displaced by 1.1 Å, accommodating the cyclopropyl group of **5**, however, it remains within H-bonding distance of Tyr912S. In contrast to HRas, SOS residues are unperturbed upon binding of **5**.

Synthesis of analogues of **5** led to acylsulfonamide **6** (**Fig. 3b**). Similar interactions are seen with Leu6R, Asp54R, and His911S. Compared with **5**, the distance between Thr74R and the S=O group of **6** increases to a range no longer conducive to hydrogen bonding. Lys5R rotates and moves ~4 Å. However, most notable is the movement of Tyr71R, which flips from the position observed in the unbound structure, where it forms a tyrosine bridge with Tyr912S, to an alternative location at the back of the pocket. This likely results from the increased steric bulk of the piperidinone ring of **6** compared with the isopropyl of **5**. The Tyr71R phenol OH moves 8.1 Å, opening up a new cavity which is occupied by a number of water molecules. **Figure 3c** shows the wide range of movement observed for the Tyr71R side chain amongst Ras structures. In unbound KRas (brown) the phenol group overlaps with site B. In the HRas (dark green):SOS (lilac) complex, Tyr71R forms a tyrosine bridge with Tyr912S and creates a pocket

between the two proteins into which compounds such as **5** may bind. Increasing the size of the small molecule ligand, such as in **6** (grey), is accompanied by further movement of Tyr71R (light green), opening up a larger binding pocket between the two proteins. Disruption of the HRas:SOS tyrosine bridge does not significantly alter the binding affinity of the fragments (**Table 1**).

X-ray crystal structures of ligands binding solely to Ras have been published since the work described in this paper was completed.[5,6] Comparison of published crystal structures with that of the HRas:SOS:**5** complex shows that site B corresponds with the relatively shallow 'binding site 2' of the published fragments **7** and **8** on KRas (**Fig. 3d**). Compound **5** interacts with HRas through its acylsulfonamide motif, while the corresponding space is left unoccupied by **7** and **8**, which instead extend beyond the confines of site B and place polar groups in the spaces occupied by Tyr912S and His911S in the HRas:SOS complex. The resulting steric clash with SOS seems likely to contribute to the inhibition of nucleotide exchange that has been reported for **8**.[6]

The challenge of obtaining biological activity

While we demonstrated binding of fragments at sites A and B by X-ray crystallography, and were able to quantify their binding affinities by NMR, this did not translate into a measurable effect on nucleotide exchange (*vide infra*). This was not surprising, since we anticipated more potent compounds would be required to show functional activity. We synthesized analogues of **1** and **5**, varying both substituents of the sulfonamide. The most interesting compound identified was **6**, where the site B binding pocket was expanded. We also made analogues of triazine **3**, varying the heteroatoms in the triazine ring, switching the thiomethyl group, and varying the piperazine side chain. We found that the basicity of the piperazine ring was critical to maintain the high levels of solubility required for screening and crystallization at high concentrations. However, after several rounds of chemistry optimization, we were unable to improve the affinity of these hits significantly or demonstrate that such small ligands were measurably able to stabilize the Ras:SOS complex.

A growing body of literature suggests that use of a ligand which binds covalently to a protein target may offer a way to permanently deactivate protein function.[7,8,17,18,19] Considering the picomolar affinity of Ras for GDP, we hypothesised that an irreversible inhibitor may afford the only realistic chance of inhibiting GTPase activity. We identified Cys118R in the HRas:SOS complex as a potentially reactive protein side chain proximal to the GDP

binding site on HRas (site C in **Fig. 1**) and set out to discover fragments which would irreversibly bind to it. This cysteine residue is conserved between HRas and KRas.

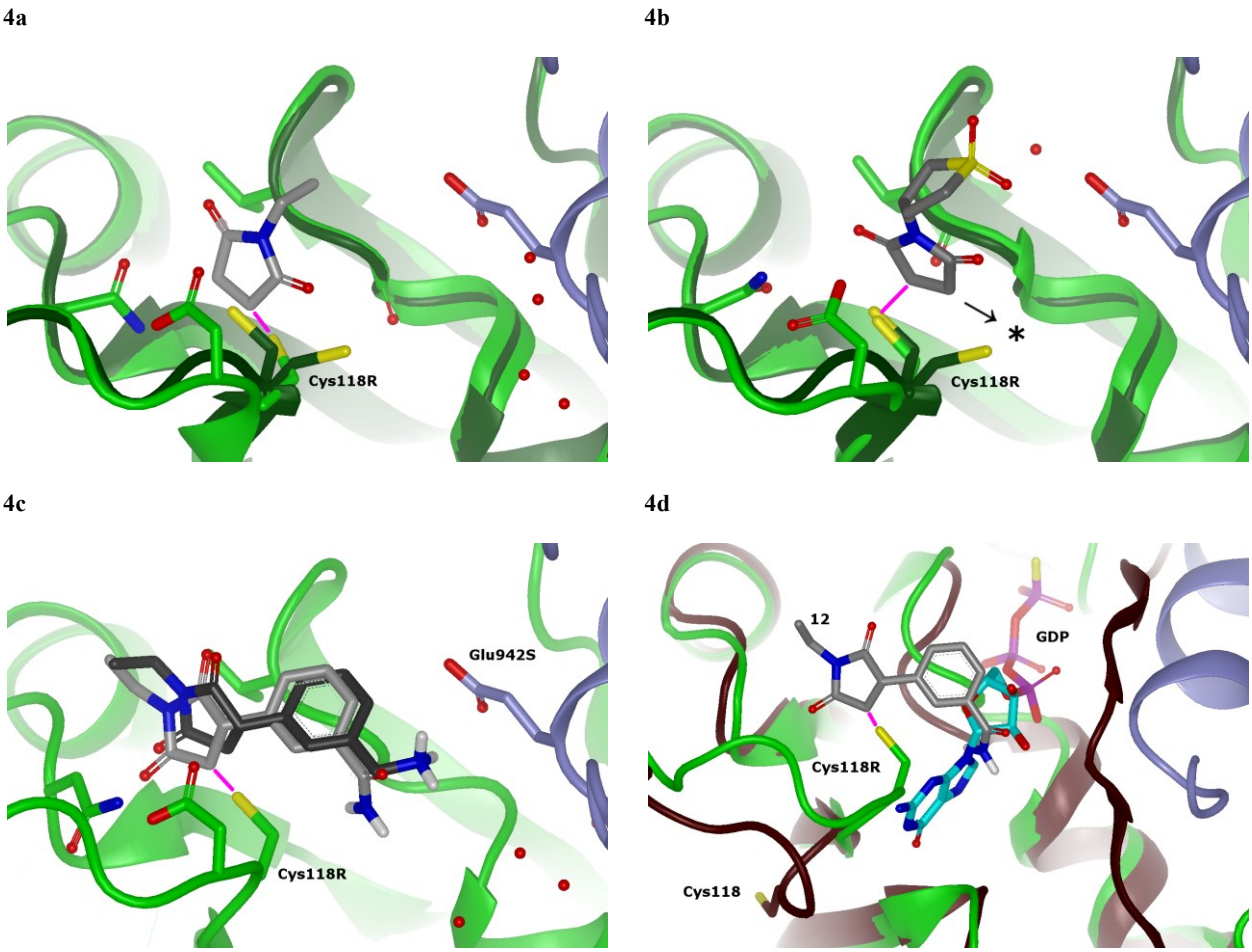

Figure 4 | Fragments binding at HRas:SOS site C. HRas colored green, SOS lilac. Where side chain movements occur on ligand binding, the relevant side chains from the HRas:SOS unbound structure *1BKD* are shown in dark green for comparison. (**a**) Covalent binding of **9** (represented by a magenta line) restrains the otherwise flexible side-chain of Cys118R into a single conformation. (**b**) Covalent binding of **10** causes Cys118R to adopt a different side-chain rotamer to that observed on binding of **9**, allowing the targeting of a new growth vector, marked by *. (**c**) The *meta*-substituents of **11** (dark grey) and **12** (light grey) follow a similar path down a lipophilic channel on Ras. (**d**) Overlay of HRas:SOS (green/lilac) in complex with **12** (grey) on the PDB KRas structure *4DSO* shows that **12** occludes the GDP (cyan) binding site on KRas (brown). A dramatic shift is seen in the position of Cys118 of KRas compared with Cys118R of the HRas:SOS:**12** complex.

Irreversible binders at HRas:SOS site C

A library of 400 compounds was selected, comprising members with fragment-like properties[20] (MWt ≤ 300, cLogP 1-3, cLogD -1 to 3, ≤ 2H-bond donors, ≤ 6 H-bond acceptors, ≤ 2rings, ≤ 6 rotatable bonds and ≤ 20 heavy atoms) and potentially reactive functional groups. These were identified from reports in the literature[21] and by mining the data from an in-house glutathione reactivity assay,[22] in which compounds with half-lives in the range of 15-3000 minutes were judged to be suitably reactive. Typical chemotypes represented in the library are shown in **Table 2**. Compounds were screened by mass spectrometry, by observing the mass increase of the HRas:SOS complex following compound addition.

We selected the reactive *N*-ethylmaleimide (NEM) group as an ideal electrophilic 'warhead' to bind to Cys118R. Other warheads were deemed either insufficiently reactive (giving incomplete cysteine adduction) or too reactive (reaction with multiple cysteine or histidine residues on the HRas:SOS complex) to progress. Using X-ray crystal structures of the HRas:SOS:inhibitor complex to guide design, we anticipated that building constructive non-covalent binding interactions with the protein (*i.e.* increasing K_i) might allow replacement of the maleimide with a less reactive motif (*i.e.* reducing K_{inact}) whilst retaining overall inhibitory activity.[23] Substitution of the maleimide double bond offered the possibility of modulating the electrophilicity of the Michael acceptor warhead, once additional non-covalent interactions had been identified.

Promising hits from the mass spectrometry screen of reactive fragments included *N*-substituted maleimides **9** and **10**. X-ray crystal structures obtained subsequently showed **9** (**Fig. 4a**) and **10** (**Fig. 4b**) binding with a distance of 1.8 Å between the ligand C-3 and the Cys118R sulfur atom, and continuous electron density, confirming that a covalent bond is formed between ligand and protein (**Supplementary Fig. 1**). Interestingly, the pyrrolidine-2,5-dione rings in **9** and **10** were observed to adopt different orientations. The C-4 atom in **10** presented an ideal vector for growing the fragment into a lipophilic channel (indicated with * in **Fig. 4b**), and a set of analogues was synthesized to vary at this position. Analogues **11** and **12**, which carry a *meta*-substituted phenyl ring at C-4, were successfully crystallized with HRas:SOS, adopting similar binding modes in which the C-4 substituent extends down a lipophilic groove adjacent to Glu942S (**Fig. 4c**). With a *meta*-substituent effectively anchoring the pendant phenyl group in one orientation, compounds **13** and **14** were designed to probe interactions with Glu942S, *via* a *bis*-3,5-substituted ring.

Comparison of the published KRas:GDP crystal structure *4DSO* and our HRas:SOS structures shows reorganization of the GDP binding pocket following association of Ras and SOS (**Fig. 4d**). This reconfiguration involves Cys118R, which is otherwise buried in the interior of the KRas:GDP complex where it may be somewhat protected from electrophiles. When SOS binds to Ras and displaces GDP, the Cys118R residue is exposed to solvent, rendering it more vulnerable to reaction with **9**-**14**. Once such a reaction has occurred, the covalently-bound fragment partly occludes the nucleotide binding site and could potentially also prevent reorganization of the Cys118R loop of Ras, thus locking the protein into the catalytically inactive Ras:SOS complex.

As we had hoped, fragments which covalently modified HRas in the crystal environment also demonstrated functional activity in preventing wild type KRas activation. Due to the spectral properties of these compounds it was not always possible to use previously-reported methods for monitoring nucleotide exchange with MANT-labeled GDP[6] as many of the compounds interfered with the excitation/emission spectra. Therefore, a novel homogeneous time-resolved fluorescence (HTRF) assay was designed to profile this series. In this homogenous assay, biotin-KRas:GDP was labeled with streptavidin europium and GST-Raf was labeled with anti-GST XL665. Activation of KRas was initiated with the addition of SOS and GTPγS. Upon binding of the active GTPγS-bound streptavidin:biotin-KRas to Raf-GST:Anti-GST XL665, the europium donor and XL665 acceptor are brought into close proximity resulting in an increased acceptor emission at 665 nm (**Supplementary Fig. 2**).

Compounds **10**-**14** were pre-incubated with either KRas:GDP, SOS alone or a KRas:GDP:SOS mixture for 2.5 hours to allow the compound to react, then inactivated by the addition of dithiothreitol (DTT). All samples were then made up to contain the same concentrations of KRas:GDP and SOS, and incubated with streptavidin-europium for 4 hours. In a separate reaction GST-Raf was incubated with anti-GST XL665. The exchange reaction was initiated by the addition of GTPγS and GST-Raf. The activation of KRas was then monitored via HTRF between the streptavidin-europium and XL665 upon binding of active KRas to GST-Raf.

Complete inhibition of KRas activation was achieved only when **10**-**14** were pre-incubated with KRas:GDP:SOS (**Fig. 5**), which supports the hypothesis that Cys118R becomes more accessible during the conformational changes which occur during SOS-mediated nucleotide exchange. Neither pre-incubation of **11**-**13** with KRas:GDP with subsequent addition of SOS nor pre-incubation with SOS followed by addition of KRas:GDP led to significant inhibition of the Ras-Raf interaction. A modest degree of KRas inhibition (~40-50%) was observed when **10** and **14** were pre-mixed with KRas alone. This may be due to the increased reactivity of the Michael

acceptors in these molecules causing them to behave in a less specific manner, as we had observed during the initial irreversible fragment screening campaign; **10** is an unsubstituted maleimide and **14** has two strong electron withdrawing groups on its phenyl ring. The inhibitory effects of **10-14** could be eliminated by the addition of DTT (1 mM) during the pre-incubation step, presumably because DTT reacted with the maleimide warhead before it was able to irreversibly modify the KRas:SOS complex.

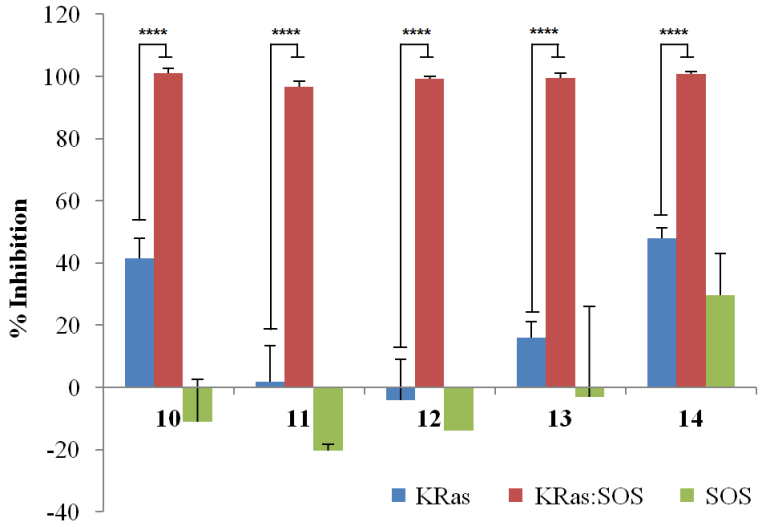

Figure 5 | Inhibition of KRas:SOS functional activity by irreversible inhibitors. Compounds **10-14** (200 µM) were pre-incubated with either GDP-loaded Biotin-KRas alone (blue), GDP-loaded biotin-KRas plus SOS (red) or SOS alone (green). All samples were then made up to contain the same concentrations of KRas:GDP and SOS. **10-14** caused complete inhibition of functional activity when pre-mixed with KRas:GDP and SOS together, but modest or no inhibition when pre-mixed with KRas:GDP or SOS alone. No inhibition was observed with non-covalent compounds **1**, **3** or **5** (data not shown). Error bars show one standard deviation. Comparison of KRas and KRas:SOS data using the unpaired T-test shows all results to be statistically significant, $p<0.0001$ (****). Full data are shown in **Supplementary Table 2**.

Site C irreversible binders show time-dependent inhibitory activity against both wild type and mutant KRas

The inactivation of wild type KRas, KRas(G12V) and KRas(G12C) was monitored using a MANT-dGDP assay and a fluorescence assay-compatible compound, **12**. Initially, the KRas constructs were pre-equilibrated with MANT-dGDP to replace the bound unlabelled nucleotide which co-purifies with KRas. All three constructs then underwent SOS-mediated nucleotide exchange which resulted in an increase in fluorescence upon MANT-dGDP binding. At

equilibrium, the reaction cycled between the MANT-dGDP and the unlabelled nucleotide. Upon the addition of **12** (200 μM), time dependent inactivation of each of the KRas constructs was observed (**Fig. 6**). An excess amount of unlabelled GDP was included as a control to compete with the MANT-dGDP resulting in a loss of fluorescence. Since the rate of reduction of fluorescence is similar with the addition of either excess GDP or irreversible inhibitor **12**, this supports the hypothesis that nucleotide exchange is driven in both cases by the rate of association of Ras:SOS. If excess GDP is present, SOS associates with Ras, the MANT-dGDP is displaced, and is then replaced with unlabelled GDP when SOS dissociates. If **12** is present when SOS associates with Ras and displaces MANT-dGDP, the resulting KRas:SOS, KRas(G12V):SOS or KRas(G12C):SOS complex reacts with the irreversible inhibitor at Cys118R, forming a dead-end complex which prevents the subsequent re-binding of MANT-dGDP.

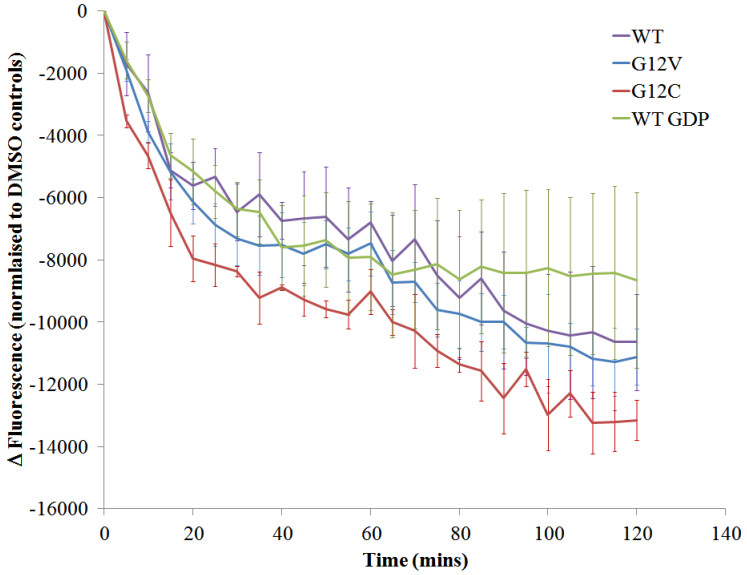

Figure 6 | Inhibition of SOS-mediated MANT-labelled nucleotide exchange by 12 in a range of Ras mutants. KRas wild type, KRas(G12V) and KRas(G12C) were equilibrated with MANT-dGDP which is environmentally sensitive and significantly increases in fluorescent quantum yield when protein bound. **12** was added (200 μM) and inactivation was monitored over time. A reduction in fluorescence was observed against all three KRas constructs (red, blue and purple lines). An excess of GDP was used as a control to compete off the MANT-dGDP (green line). Color-coded error bars for measurements are also shown. Full data are shown in **Supplementary Table 3**.

DISCUSSION AND CONCLUSIONS

Our work with non-covalent fragments showed that it was possible to characterize compounds from multiple series binding on SOS and at the HRas:SOS interface, however, none of these compounds were sufficiently potent to show

functional activity in the Ras:Raf HTRF assay. Synthesis of analogues of **1**, **3**, **5** and **6** led to compounds with similar binding affinities to the parent fragments and unproductive SAR. The report by Burns *et al.* that small molecules which bind at SOS site A cause an increase in the rate of SOS-mediated nucleotide exchange[11] was not corroborated by experiments with our fragments, suggesting that more dramatic changes or hybridization of series may be required to achieve sufficient binding affinity. While we were not able to detect functional biological activity for the probes identified at sites A and B, we believe that our observations of specific ligandable[24] interaction points may suggest a potential way forward using larger molecules such as macrocycles[25] or constrained peptides.[26] The distance between the closest atoms on non-covalent fragments bound in sites A and B is 9.1 Å. Precedent for linking distant fragment sites suggests that connecting two weak fragments can bring very large increases in potency, but is most likely to succeed when fragments are significantly closer together than sites A and B. If fragment ligands for sites A and B could be iteratively grown towards each other, however, this strategy may be more likely to succeed.[27]

While our efforts to inhibit Ras by stabilization of the Ras:SOS complex by fragments binding in a reversible manner were unsuccessful, we showed that reactive fragments which covalently modify site C near to the nucleotide binding site were effective Ras inhibitors. We demonstrated complete inhibition of KRas:SOS functional activity following reaction of maleimides **10**-**14** with Cys118R, a previously undescribed method of inhibition of Ras. A synthetic chemistry campaign led to fragments which showed a consistent binding mode at site C, and resulted in inhibition of wild type KRas in a novel HTRF assay measuring the Ras-GTP:Raf interaction. Several potential vectors were identified for further growth of these inhibitors; for example, along the lipophilic channel from the *meta* position of phenyl groups in **11**-**14**, or from the maleimide *N*-substituent towards SOS.

An important objective for a covalent approach to Ras:SOS inhibition is to reconcile the need to measure variations in potency of molecules – and hence structure-activity relationships – with the requirement for a warhead of high reactivity necessary to observe any inhibitory activity. With the fragment series based on maleimides, although it was possible to measure potency and inhibition of nucleotide exchange, this measure was driven largely by K_{inact}, and small changes in K_i were difficult to detect. The determination of K_i changes is important to assist the design of more potent, but less reactive inhibitors. Tuning the reactivity of the covalent modifier by modulating the electrophilicity of the Michael acceptor warhead could potentially be achieved by using an electron-donating linker such as ether or amine. Kathman *et al.* recently published an example of this approach being used successfully against a cysteine protease.[28]

Our work has explored three small molecule binding sites on the Ras:SOS complex, and details synthetically accessible small molecule probes that bind at each site. We demonstrated inhibition of KRas functional activity with compounds which bind irreversibly at site C, and showed that covalent binding with HRas in a protein crystal environment translates to nucleotide exchange inhibition in the more oncology disease-relevant isoform KRas. Furthermore, this mechanism of KRas inactivation appears to be applicable to mutant forms of KRas which also share a Cys118 residue, such as KRas(G12C) and KRas(G12V). Although significant work remains to optimize the biological activity of the compounds we have described at site C, our discoveries open the way to a new strategy to target aberrant Ras signalling by intervening in the SOS-mediated activation of Ras.

ANCILLARY INFORMATION

Supporting Information Available: Experimental methods and any associated references are available in the online version of this paper. This material is available free of charge via the Internet at http://pubs.acs.org.

PDB ID codes: 4URU, 4URV, 4URW, 4URX, 4URX, 4URY, 4URZ, 4US0, 4US1, 4US2.

Corresponding Author Information: Jon Winter (jon.winter@astrazeneca.com)

Competing financial interests: All authors are or were employees and stockholders of AstraZeneca Inc.

Acknowledgements: We dedicate this paper to the memory of J. Andrew Grant, whose shape-matching algorithms assisted us greatly. The authors also thank Ian Sinclair, John Cuff and James Haigh for building a library of cocktailed fragments, and both the European Synchrotron Radiation Facility, Grenoble and Diamond Light Source, Oxfordshire for access to beam time.

Author Contributions: J.J.G.W. designed the fragment libraries and compounds, analyzed data, supervised the chemistry team and wrote the manuscript. M.A. designed and performed mass spectrometry experiments and analyzed data. A.L.B. designed the research plan and wrote the manuscript. K.B., G.F., P.P. & G.W. designed synthetic chemistry routes, synthesized and characterized compounds. C.B. designed and performed protein crystallization experiments. C.C. designed biological experiments. K.E. performed K_D determinations via biomolecular NMR. P.F. & L.S. provided computational support for fragment library and compound design. M.R.V.F. analyzed data, designed compounds, supervised the chemistry team and wrote the manuscript. J.G.K. conceived the target hypothesis, oversaw the project team and wrote the manuscript. T.N. analyzed data and designed compounds. R.O. designed, expressed and purified protein constructs. S.J.P. purified proteins, designed,

performed and interpreted X-ray crystallography experiments and designed compounds. J.T. designed and performed biological experiments. J.A.T. designed, performed and interpreted X-ray crystallography experiments and designed compounds.

REFERENCES

1. Karnoub, A. E.; Weinberg, R. A. Ras oncogenes: split personalities. *Nat. Rev. Mol. Cell Biol.* **2008**, *9*, 517-531.
2. Spiegel, J.; Cromm, P. M.; Zimmermann, G.; Grossmann, T. N.; Waldmann, H. Small-molecule modulation of Ras signalling. *Nat. Chem. Biol.* **2014**, *10*, 613-622.
3. Rusconi, P.; Caiola, E.; Broggini, M. RAS/RAF/MEK inhibitors in oncology. *Curr. Med. Chem.* **2012**, *19*, 1164-1176.
4. Shutes, A.; Onesto, C.; Picard, V.; Leblond, B.; Schweighoffer, F.; Der, C. J. Specificity and mechanism of action of EHT 1864, a novel small molecule inhibitor of Rac family small GTPases. *J. Biol. Chem.* **2007**, *282*, 35666-35678.
5. Sun, Q.; Burke, J. P.; Phan, J.; Burns, M. C.; Olejniczak, E. T.; Waterson, A. G.; Lee, T.; Rossanese, O. W.; Fesik, S. W. Discovery of small molecules that bind to K-Ras and inhibit Sos-mediated activation. *Angew. Chem. Int. Ed.* **2012***, 51*, 6140-6143.
6. Maurer, T.; Garrenton, L. S.; Oh, A.; Pitts, K.; Anderson, D. J.; Skelton, N. J.; Fauber, B. P.; Pan, B.; Malek, S.; Stokoe, D.; Ludlam, M. J.; Bowman, K. K.; Wu, J.; Giannetti, A. M.; Starovasnik, M. A.; Mellman, I.; Jackson, P. K.; Rudolph, J.; Wang, W.; Fang, G. Small-molecule ligands bind to a distinct pocket in Ras and inhibit SOS-mediated nucleotide exchange activity. *Proc. Natl. Acad. Sci. USA* **2012***, 109*, 5299-5304.
7. Ostrem, J. M.; Peters, U.; Sos, M. L.; Wells, J. A.; Shokat, K. M. K-Ras(G12C) inhibitors allosterically control GTP affinity and effector interactions. *Nature* **2013**, *503*, 548-551.
8. Lim, S. M.; Westover, K. D.; Ficarro, S. B.; Harrison, R. A.; Choi, H. G.; Pacold, M. E.; Carrasco, M.; Hunter, J.; Kim, N. D.; Xie, T.; Sim, T.; Jänne, P. A.; Meyerson, M.; Marto, J. A.; Engen, J. R.; Gray, N. S. Therapeutic targeting of oncogenic K-Ras by a covalent catalytic site inhibitor. *Angew. Chem. Int. Ed. Engl.* **2014**, *53*, 199-204.
9. Renault, L.; Guibert, B.; Cherfils, J. Structural snapshots of the mechanism and inhibition of a guanine nucleotide exchange factor. *Nature* **2003**, *426*, 525-530.

10. Peyroche, A.; Antonny, B.; Robineau, S.; Acker, J.; Cherfils, J.; Jackson C. L. Brefeldin A acts to stabilize an abortive ARF-GDP-Sec7 domain protein complex: Involvement of specific residues of the Sec7 domain. *Mol. Cell* **1999**, *3*, 275–285.
11. Burns, M. C.; Sun, Q.; Daniels, R. N.; Camper, D.; Kennedy, J. P.; Phan, J.; Ojejniczak, E. T.; Lee, T.; Waterson, A. G.; Rossanese, O. W.; Fesik, S. W. Approach for targeting Ras with small molecules that activate SOS-mediated nucleotide exchange. *Proc. Natl. Acad. Sci. USA* **2014**, *111,* 3401-3406.
12. Boriack-Sjodin, P. A.; Margarit, S. M.; Bar-Sagi, D.; Kuriyan, J. The structural basis of the activation of Ras by Sos. *Nature* **1998**, *394*, 337-343.
13. Bosch, J.; Robien, M. A.; Mehlin, C.; Boni, E.; Riechers, A.; Buckner, F. S.; Van Voorhis, W. C.; Myler, P. J.; Worthey, E. A.; DeTitta, G.; Luft, J. R.; Lauricella, A.; Gulde, S.; Anderson, L. A.; Kalyuzhniy, O.; Neely, H. M.; Ross, J.; Earnest, T. N.; Soltis, M.; Schoenfeld, L.; Zucker F.; Merritt E. A.; Fan E.; Verlinde C. L.; Hol W. G. Using fragment cocktail crystallography to assist inhibitor design of *Trypanosoma brucei* nucleoside 2-deoxyribosyltransferase. *J. Med. Chem.* **2006**, *49*, 5939-5946.
14. Margarit, M. S.; Sondermann H.; Hall, B. E.; Nagar, B.; Hoelz, A.; Pirruccello, M.; Bar-Sagi, D.; Kuriyan, J. Structural evidence for feedback activation by Ras·GTP of the Ras-specific nucleotide exchange factor SOS. *Cell* **2003**, *112*, 685-695.
15. Haigh, J. A.; Pickup, B. T.; Grant, J. A.; Nicholls, A. Small molecule shape-fingerprints. *J. Chem. Inf. Model.* **2005**, *45*, 673-684.
16. Protein subunit nomenclature: Leu6R refers to leucine 6 on the Ras protein chain, and His911S refers to histidine 911 on SOS.
17. Kalgutkar, A. S.; Dalvie, D. K. Drug discovery for a new generation of covalent drugs. *Expert Opin. Drug Discov.* **2012**, *7*, 561-581.
18. Johnson, D. S.; Weerapana, E.; Cravatt, B. F. Strategies for discovering and derisking covalent, irreversible enzyme inhibitors. *Future Med. Chem.* **2010**, *2*, 949-964.
19. Mah, R.; Thomas, J. R.; Shafer, C. M. Drug discovery considerations in the development of covalent inhibitors. *Bioorg. Med. Chem. Lett.* **2014**, *24*, 33-39.
20. Congreve, M.; Carr, R.; Murray, C.; Jhoti, H. A 'rule of three' for fragment-based lead discovery? *Drug Discov. Today* **2003**, *8,* 876-877.

21. Potashman, M. H.; Duggan, M. E. Covalent modifiers: An orthogonal approach to drug design. *J. Med. Chem*. **2009**, *52*, 1231-1246.
22. MacFaul, P. A.; Morley, A. D.; Crawford, J. J. A simple in vitro assay for assessing the reactivity of nitrile containing compounds. *Bioorg. Med. Chem. Lett.* **2009**, *19*, 1136-1138.
23. Ward, R. A.; Anderton, M. J.; Ashton, S.; Bethel, P. A.; Box, M.; Butterworth, S.; Colclough, N.; Chorley, C. G.; Chuaqui, C.; Cross, D. A. E.; Dakin, L. A.; Debreczeni, J. É.; Eberlein, C.; Finlay, M. R. V.; Hill, G. B.; Grist, M.; Klinowska, T. C. M.; Lane, C.; Martin, S.; Orme, J. P.; Smith, P.; Wang, F.; Waring, M. J. Structure- and reactivity-based development of covalent inhibitors of the activating and gatekeeper mutant forms of the Epidermal Growth Factor Receptor (EGFR). *J. Med. Chem.* **2013**, *56*, 7025-7048.
24. Edfeldt, F. N.; Folmer, R. H. A.; Breeze, A. L. Fragment screening to predict druggability (ligandability) and lead discovery success. *Drug Discov. Today* **2011**, *16*, 284-287.
25. Giordanetto, F.; Kihlberg, J. Macrocyclic drugs and clinical candidates: What can medicinal chemists learn from their properties? *J. Med. Chem.* **2014**, *57*, 278-295.
26. Henchey, L. K.; Jochim, A. L.; Arora, P. S. Contemporary strategies for the stabilization of peptides in the α-helical conformation. *Curr. Opin. Chem. Biol.* **2008**, *12*, 692-697.
27. Ward, R. A.; Brassington, C.; Breeze, A. L.; Caputo, A.; Critchlow, S.; Davies, G.; Goodwin, L.; Hassall, G.; Greenwood, R.; Holdgate, G. A.; Mrosek, M.; Norman, R. A.; Pearson, S.; Tart, J.; Tucker, J. A.; Vogtherr, M.; Whittaker, D.; Wingfield, J.; Winter, J.; Hudson, K. Design and synthesis of novel lactate dehydrogenase A inhibitors by fragment-based lead generation. *J. Med. Chem.* **2012**, *55*, 3285-3306.
28. Kathman, S. G.; Xu, Z.; Statsyuk, A. V. A fragment-based method to discover irreversible covalent inhibitors of cysteine proteases. *J. Med. Chem.* **2014**, *57*, 4969-4974.

TABLES

Compound	**Structure**	**HRas:SOS NMR binding K_D mM (std.err.)**	**Binding site**	**Protein Data Bank Accession Code**

1	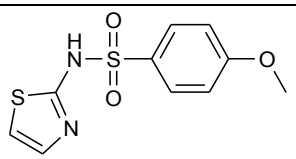	6.0 (±6.0)[a]	A	*4URU*
2	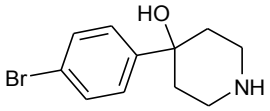	1.7 (±0.2)	A	*4URV*
3	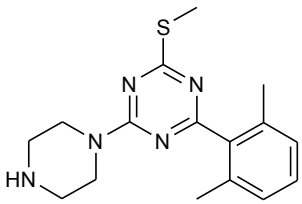	1.6 (±0.1)	A	*4URW*
4a	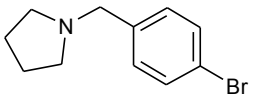	1.3 (±0.2)	A[b]	*4URX*
4b	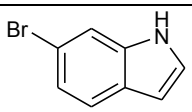	6.0 (±3.0) [a]	A[b]	*4URX*
5	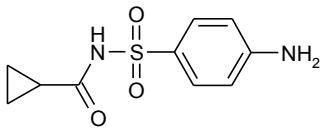	6.0 (±2.0)	B	*4URY*
6	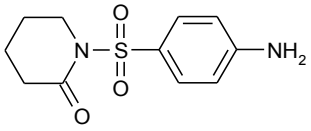	3.0 (±0.4)	B	*4URZ*
7	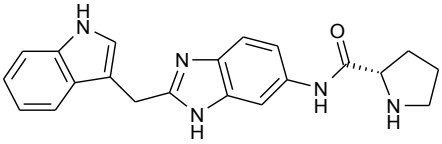	nd[c]	KRas site 2[d]	*4EPY*
8	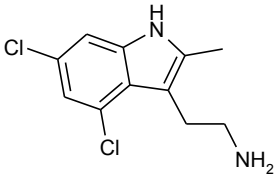	nd[c]	KRas site 2[e]	*4DST*

9	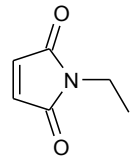	nd[c]	C	*4US0*
10	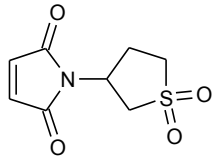	nd[c]	C	
11-14	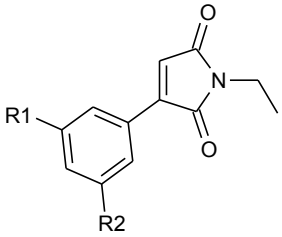			
11	$R1 = CH_2NH_2$ R2 = H	nd[c]	C	*4US1*
12	$R1 = CONH_2$ R2 = H	nd[c]	C	*4US2*
13	R1 = COOH R2 = CN	nd[c]	C	
14	$R1 = CONH_2$ R2 = Cl	nd[c]	C	

Table 1 | Structure and NMR binding K_D of HRas:SOS ligands. The crystal structures for HRas:SOS:compound complexes are deposited in the Protein Data Bank (PDB, http://www.rscb.org) under the accession codes above. Values for K_D determined by NMR chemical shift mapping are shown with the standard error of the mean for each measurement. [a] Significant precipitation was observed. [b] **4a** and **4b** only bound when both ligands were present in the same cocktail. [c] K_D measurements were not generated for the literature compounds **7** & **8**, which bind to Ras alone, or covalently bound compounds **9 – 14**. [d] See reference 5. [e] See reference 6.

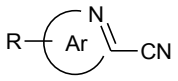	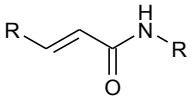	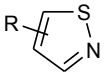	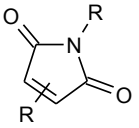
Heteroaryl nitrile[a]	Vinyl amide[a]	Isothiazole[b]	Maleimide[b]
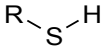	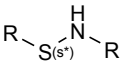	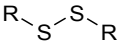	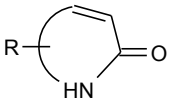
Thiol[a]	Sulfanylamino[b]	Disulfide[a]	Vinyl lactam[b]

Table 2 | Examples of reactive functional groups represented in the covalent fragment library. R indicates any functional group.[a] See reference 21. [b] See reference 22.

Table of contents graphic

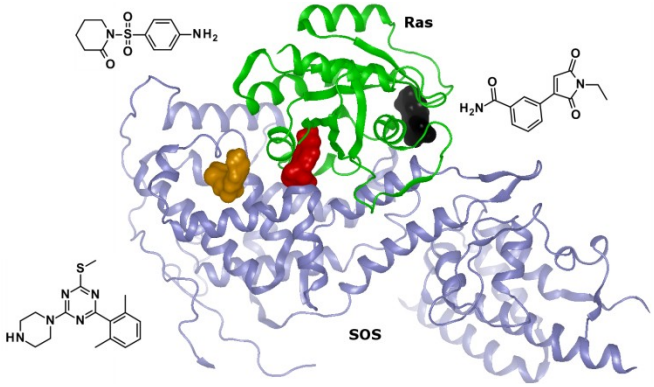

Small molecule binding sites on the Ras:SOS complex can be exploited for inhibition of Ras activation

Jon J. G. Winter,[a,*] Malcolm Anderson,[a,b] Kevin Blades,[a] Claire Brassington,[a] Alexander L. Breeze,[a,c] Christine Chresta,[a] Kevin Embrey,[a] Gary Fairley,[a] Paul Faulder,[a,d] M. Raymond V. Finlay,[a] Jason G. Kettle,[a] Thorsten Nowak,[a,e] Ross Overman,[a] S. Joe Patel,[a,f] Paula Perkins,[a,g] Loredana Spadola,[a] Jonathan Tart,[a] Julie A. Tucker[a,h] & Gail Wrigley[a]

[a] AstraZeneca, Alderley Park, Macclesfield, Cheshire, SK10 4TG, United Kingdom. * Author to whom correspondence should be addressed (email: jon.winter@astrazeneca.com). *Present Author Addresses*: [b] Waters Corporation, Atlas Park, Simonsway, Manchester, M22 5PP, United Kingdom (M.A.); [c] Astbury Centre for Structural Molecular Biology, University of Leeds, Leeds, LS2 9JT, United Kingdom (A.L.B.); [d] Elixir Software Ltd., Lynwood House, Rowton Lane, Rowton, Chester, Cheshire, CH3 6AT, United Kingdom (P.F.); [e] C4X Discovery Ltd., Unit 310 Ducie House, Ducie Street, Manchester, M1 2JW, United Kingdom (T.N.); [f] AstraZeneca, Gatehouse Park, 35 Gatehouse Drive, Waltham, MA 02451, USA (S.J.P.); [g] 45 Sycamore Crescent, Macclesfield, Cheshire, SK11 8LW, United Kingdom (P.P.); [h] Northern Institute for Cancer Research, Paul O'Gorman Building, Newcastle University, Framlington Place, Newcastle upon Tyne, NE2 4HH, United Kingdom (J.A.T.).

SUPPORTING INFORMATION

TABLE OF CONTENTS

References

Nuclear magnetic resonance K_D determinations. Samples of 6His-TEV-SH-HRas(1-166) and 6His-TEV-SH-SOS uniformly labeled with $^{2}H,^{15}N$ were produced in *E. coli* using M9 minimal media supplemented with 5 g/L Celtone base powder (^{2}H, 97%, ^{15}N, 98%; Cambridge Isotope Laboratories Inc.), yielding 15 and 150 mg/L of purified protein, respectively. The purification was via NiNTA, TEV cleavage and dialysis, subtractive NiNTA to remove the tag and size exclusion chromatography (SEC) using a Superdex 200 column. After cleavage, both proteins were left with GSH residues preceding the protein sequence. A 16-fold excess of GTPγS was added to the HRas sample to achieve exchange of bound nucleotide, and was then left at room temperature overnight to equilibrate before passing down a PD10 column to remove excess nucleotide. The 2:1 HRas:SOS complex was formed by adding HRas(GTPγS) and SOS from concentrated stocks (~0.8 mM) to obtain 0.5 mL of 0.16 mM HRas and 0.08 mM SOS in 50 mM HEPES (pH 7.4), 50 mM NaCl, 2 mM TCEP, 2 mM $MgSO_4$, 0.1 mM EDTA and 0.02 % NaN_3. NMR spectra were collected at 298 K on a Bruker Avance 600 MHz spectrometer running TopSpin 2.1, equipped with a 5 mm TCI Cryoprobe with Z-axis gradients. The complex was titrated with compound stocks (typically at 200 mM) to give final compound concentrations of 0, 0.2, 0.6, 1.4, 3.4 and 7.4 mM; these were measured using 2D $^{1}H,^{15}N$-TROSY-HSQC[29] experiments recorded with 2048x50 (t_2,t_1) complex points (in Echo-Antiecho mode), and 12019x2068 Hz ($^{1}H,^{15}N$) spectral widths, (85.3 ms x 24.2 ms acquisition times, respectively). The affinity of the compounds was determined via simultaneous nonlinear fitting of fast-exchange chemical shift perturbations (typically 5 amide correlations, employing the absolute value of the linear $^{1}H,^{15}N$ chemical shift vector) against compound concentration using a mass action binding isotherm equation.

Mass spectrometry analysis of covalent adduction to proteins. The HRas:SOS complex was prepared by pre-incubating the purified recombinant HRas with GTPγS (>10 fold molar excess). Both HRas and SOS proteins were transfered individually by gel filtration chromatography into ammonium acetate buffer (20 mM, pH 6.8). Their concentrations were estimated by UV absorbance at 280 nm (NanoDrop, Thermo, Wilmington, DE, USA), before combining the two protein solutions in a stoichiometric ratio of ~2:1 (Ras:SOS) to give final protein concentrations of ~19 μM and ~10 μM respectively. Fragment-like compounds were prepared as solutions at a concentration of 10 mM in either ethanol or acetonitrile. Compound solutions (180 nL) were added to protein solutions (3.25 μL) and

mixed using 10 cycles of aspiration and re-dispensing (Mosquito HTS, TTPLabtech, Hertfordshire, UK). Incubation (2 hours at room temperature) was in sealed 384-well plates. Automated analysis was performed by sampling directly from the incubation plate and infusing using an Advion Nanomate (Advion, Ithaca, NY, USA) mounted on the source of a QToF mass spectrometer (QToF Micro, Waters, Manchester, UK). Data acquisition (~2 minutes) for each sample was initially under non-denaturing ionisation conditions, changing to denaturing conditions approximately halfway through the acquisition. Data were interpreted manually. Those data obtained under denaturing conditions detected quantitative covalent adduction of compound to the individual HRas and SOS subunits. Any observed delta mass increase was calculated (multiplying the Δ m/z by the protein charge state) and validated by comparison with the expected mass increase resulting from the predicted reaction mechanism of the compound. Data obtained under non-denaturing conditions detected covalent adduction, and also modulation of the protein complex quantitative distribution.

Crystallographic system. A dual expression vector encoding HRas 1-166 with an N-terminal TEV protease cleavable hexa-histidine tag and untagged SOS^{cat} 564-1049 was used to direct expression of the HRas:SOS complex in *E.coli*. Following cell lysis, the clarified lysate was batch bound to a nickel NTA resin using a buffer comprised of 40 mM HEPES (pH 8.0), 300 mM NaCl, 20 mM imidazole and 2 mM β-mercaptoethanol, and finally eluted with a step gradient of 500 mM imidazole. The eluted complex was incubated overnight in the presence of TEV protease to remove the affinity tag, whilst dialyzing against a buffer comprised of 40 mM HEPES (pH 8.0), 300 mM NaCl and 2 mM β-mercaptoethanol to reduce the imidazole concentration to 20 mM. Reverse affinity purification was performed to remove the protease and uncleaved material. This was followed with a gel filtration chromatographic step using a Superdex 200 column run in a final buffer of 20 mM TRIS (pH 8.0) and 100 mM NaCl. The peak containing the HRas:SOS complex was pooled, concentrated to 11 mg/mL, and stored at -80 °C. Protein crystallisation was performed using sitting drops at room temperature with 1:1 ratios of protein complex to a mother liquor comprised of 3.8-4.0 M sodium formate and 0.1 M TRIS (pH 8.0). Crystals appeared within a few days and grew to their final size in 1-2 weeks. Cocktail soaking was performed by transferring crystals into a solution containing 4.5 M sodium formate, 5% glycerol and a total cocktail concentration of 50 mM in 20% DMSO, representing 12.5 mM of each fragment. Following one hour exposure, crystals were harvested and frozen for data collection. For single compound soaks, a soaking solution of 4.5 M sodium formate, 0.1 M TRIS (pH 8.0) and 5% glycerol was used with a final

concentration of compound at 10 mM, 10% DMSO. Data were collected at both the European Synchrotron Radiation Facility in Grenoble, France, and Diamond Light Source, Oxford, UK. The search model used during structure solution was *1BKD*. A combination of software from the CCP4 suite[30] and the Global Phasing Consortium[31,32] was used to process the data, and solve and refine the structures. Manual model completion in Coot[33] was used to generate the final models for design. **Supplementary Figure 1** shows an example of electron density that was collected.

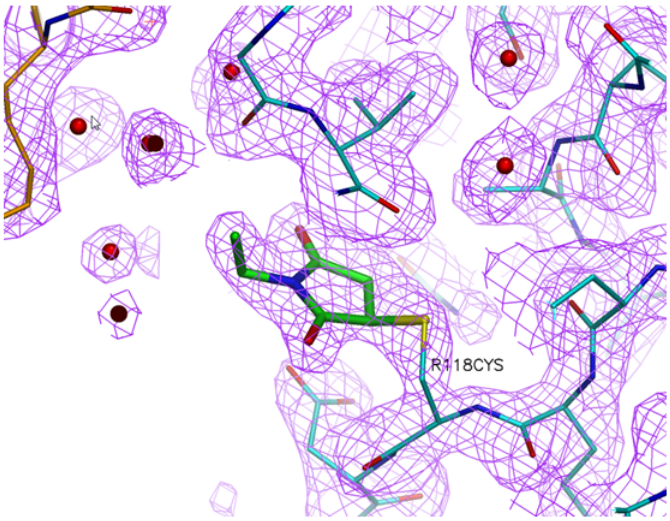

Supplementary Figure 1 | Example of electron density data collected. An example of 2Fo-Fc electron density for the covalent addition of small molecules to cysteine 118 of HRas. HRAS and SOS^{cat} are depicted with cyan and orange carbon atoms respectively. The refined final map is contoured at 1σ.

	4URU	4URV	4URW	4URX	4URY	4URZ	4US0	4US1	4US2
Data collection									
Space group	I422	I422	I422	I422	I422	I422	I422	I422	I422
Cell dimensions									
a, *b*, *c* (Å)	149.28, 149.28, 200.52	149.90, 149.90, 200.20	149.41, 149.41, 200.34	149.87, 149.87, 199.70	149.68, 149.68, 200.18	150.21, 150.21, 201.62	149.22, 149.22, 201.04	149.56, 149.56, 199.64	149.71, 149.71, 200.08
α, β, γ (°)	90, 90, 90	90, 90, 90	90, 90, 90	90, 90, 90	90, 90, 90	90, 90, 90	90, 90, 90	90, 90, 90	90, 90, 90
Resolution (Å)	120 (2.83) *	50.0 (2.58) *	120 (2.76) *	120 (2.48) *	120 (2.47) *	120 (2.24) *	120 (2.17) *	50 (2.65) *	53 (2.48) *
R_{sym} or R_{merge}	0.068 (0.478)	0.091 (0.746)	0.099 (0.503)	0.056 (0.506)	0.076 (0.489)	0.074 (0.49)	0.063 (0.479)	0.121 (0.865)	0.116 (0.759)
$I / \sigma I$	30.7 (5.6)	15.9 (2.5)	12.7 (3.3)	33.4 (5.1)	17.7 (4.6)	17.1 (3.6)	33.2 (6.4)	13.7 (2.3)	11.6 (2.5)
Completeness (%)	100 (100)	97.6 (99)	100 (100)	100 (100)	91.9 (94.7)	90.5 (91.4)	100 (100)	92.9 (94.3)	97.3 (99.0)
Redundancy	12 (12.3)	6.8 (6.9)	6.7 (6.2)	12 (11.3)	7.9 (7.8)	7.2 (7.1)	13.9 (14.1)	7.2 (7.2)	6.9 (6.8)
Refinement									
Resolution (Å)	2.83	2.58	2.76	2.49	2.47	2.25	2.17	2.65	2.48
No. reflections	27366	35039	29346	40039	37338	50173	59613	30842	39224
R_{work} / R_{free}	19.2 / 23.7	19.5 / 23.2	18.2 / 23.0	19.5 / 22.6	19.4 / 22.9	19.1 / 21.2	18.7 / 21.2	19.3 / 23.1	19.2 / 22.8
No. atoms									
Protein	5053	5034	5058	5043	5029	5065	5063	5072	5060
Ligand/ion	17	20	22	26	32	17	9	17	18
Water	71	198	201	195	183	247	493	178	301
B-factors									
Protein	60.4	54.4	46.7	55.4	54.6	54.2	42	51.4	50
Ligand/ion	76	72.9	46.2	60.2	67.4	59.3	56.2	74.9	71
Water	47.5	47.4	39.6	50.3	50.2	52.4	47.8	42.4	47.2
R.m.s. deviations									
Bond lengths (Å)	1.436	1.435	1.417	1.422	1.404	1.441	1.408	1.414	1.414
Bond angles (°)	0.015	0.014	0.014	0.014	0.014	0.014	0.014	0.014	0.014

Supplementary Table 1 | X-ray crystallographic data collection and refinement statistics. All structures were solved using data from a single crystal.
* Values in parentheses are for highest-resolution shell.

Ras:Raf HTRF assays. Reagents were diluted in 20 mM HEPES, 150 mM NaCl, 5 mM $MgCl_2$, 0.01% Tween-20 (exchange buffer) unless otherwise noted. Results are given in **Supplementary Table 2**. A graphical representation of this assay can be found in **Supplementary Figure 2**.

KRas premix variant. *A-1.* In a low volume 384 well plate (Greiner 784904) 1 µL of compound (1 mM in DMSO, 200 µM final during the pre-incubation step) was incubated with 4 µL biotinylated-KRas-GDP (15 nM in exchange buffer). The reaction was incubated for 2.5 hrs at ambient temperature and then 1 µL of streptavidin europium (Cisbio, 610SAKLB) (750 ng/mL in exchange buffer additionally containing 20 mM DTT), was added. Finally, 4 µL SOS (5 µM in exchange buffer) was added. This mixture was incubated for 4 hours to allow the detection reagents to equilibrate.

B. In a separate 1.5 mL reaction GST-Raf (20 nM) was added to with anti-GST XL665 (4 µg/mL, Cisbio, 61GSTXLA) in exchange buffer additionally containing potassium fluoride (0.1 M) and BSA (0.01% w/v). This mixture was incubated for 4 hours to allow the detection reagents to equilibrate.

C. 3 µL GTPγS (1 mM in exchange buffer) was added to sample *B* and a 10 µL sample of *B*+GTPγS was added to each well of *A-1* to initiate nucleotide exchange. Final assay concentrations were 3 nM biotin-KRas, 1 µM SOS, 1 µM GTPγS, 10 nM GST-Raf, 2 µg/mL anti-GST-XL665 and 37.5 µg/mL streptavidin europium. The plate was read after 60 minutes using an EnVision plate reader (Perkin Elmer) with an excitation wavelength of 320 nm, emission wavelengths of 615 nm and 665 nm, and the data was normalized to the donor emission (615 nm/665 nm x 10^4). An increase in the emission ratio was detected when the europium and XL665 were brought into close proximity by the binding event between activated KRas and Raf. Inhibition values were calculated from control DMSO samples containing no compound (0 % inhibition) or no biotin-KRas (100% inhibition).

KRas:SOS premix variant. *A-2*. In a low volume 384 well plate (Greiner 784904) 1 µL of compound (2 mM in DMSO, 200 µM final during the pre-incubation step) was incubated with 4 µL biotinylated-KRas-GDP (15 nM in exchange buffer) and 5 µL SOS (4 µM in exchange buffer). The reaction was incubated for 2.5 hrs at ambient temperature and then 1 µL of streptavidin europium (Cisbio, 610SAKLB) (750 ng/mL in exchange buffer additionally containing 20 mM DTT), was added. This mixture was incubated for 4 hours to allow the detection reagents to equilibrate. Mixture *B* was prepared and added to *A-2* as previously described in step *C* (*vide supra*).

SOS premix variant. *A-3.* In a low volume 384 well plate (Greiner 784904) 1 µL of compound (1 mM in DMSO, 200µM final during the pre-incubation step) was incubated with 4 µL SOS (5 µM in exchange buffer). The reaction was incubated for 2.5 hrs at ambient temperature and then 1 µL of streptavidin europium (Cisbio,

610SAKLB) (750 ng/mL in exchange buffer additionally containing 20 mM DTT), was added. Finally, 4 µL biotinylated-KRas-GDP (15 nM in exchange buffer) was added. This mixture was incubated for 4 hours to allow the detection reagents to equilibrate. Mixture *B* was prepared and added to *A-3* as previously described in step *C* (*vide supra*).

Assay statistics. The assay data varies depending on the pre-incubation conditions (*A-1*, *A-2* or *A-3*) but typical values are in the ranges shown below:

- Signal to noise = 9 – 28
- Signal to background = 2.8 – 4.3
- % CV = 3.6 – 11.5
- Z' = 0.51 – 0.83. Depending on the exact format used Z' values of >0.7 are routinely achieved.
- Range and sensitivity: The theoretical tight-binding limit for compounds targeting KRas is ~1.5 nM, and for SOS binders is 500 nM.

Comment on the high concentration of SOS. The rate of nucleotide exchange will be determined by many factors including the affinity of SOS for the nucleotide bound KRas, the rate of dissociation of GDP, association of GTP, dissociation of SOS and subsequent binding of active KRas to the Raf to generate the HTRF signal. Therefore a pragmatic approach was taken and the SOS was simply titrated into the assay and the initial rate of exchanged was monitored. The concentration selected was approximately half the maximum rate measured. This is analogous to the Km of an enzyme reaction. The 60 minute endpoint selected was on the linear part of the exchange curve. The 1 µM SOS used is not inconsistent with other groups using the MANT assay but this HTRF assay is more sensitive and enables the KRas concentration to be much lower than is required for the MANT assay.

S2a

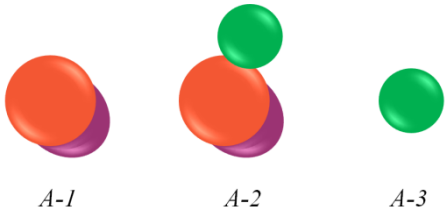

S2b

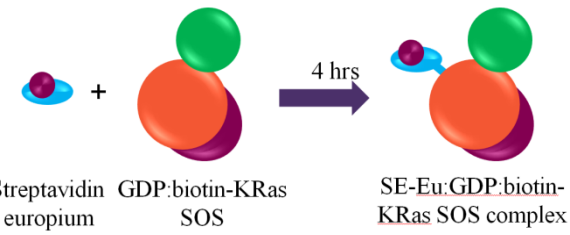

S2c

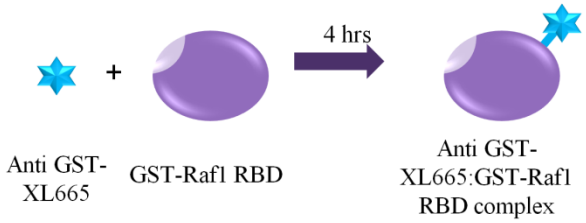

S2d

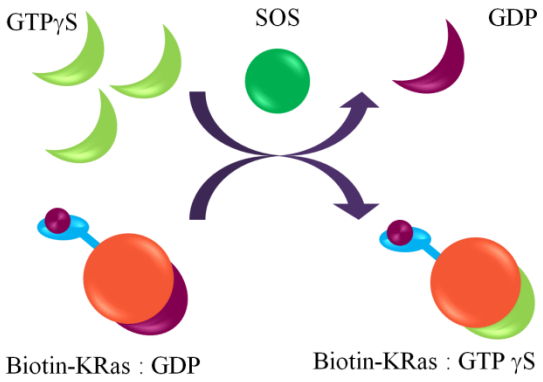

S2e

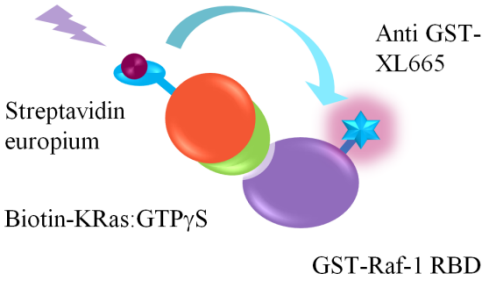

Supplementary Figure 2 | Schematic representation of the HTRF assay. (**a**) *Step A:* Compound pre-incubation. Test compounds were pre-incubated with either GDP:biotinylated KRas alone (*A-1*), GDP:biotinylated KRas + SOS (*A-2*) or SOS alone (*A-3*) for 2.5 hours. Mixtures of GDP, Ras and SOS are assumed to be in equilibrium as Ras:GDP and Ras:SOS but for simplicity are depicted as a single complex in the figure. (**b**) KRas and SOS concentrations in the three sets of pre-incubation conditions were normalized and streptavidin-europium added to each sample. (**c**) *Step B:* GST-Raf and anti-GST were mixed and incubated for 4 hours to allow the detection reagents to equilibrate. (**d**) *Step C:* KRas activation and detection. SOS-mediated nucleotide exchange and detection was initiated by the addition of the GTPγS and simultaneous addition of Raf-1/XL665. (**e**) KRas:GTPγS is detected upon binding to GST-Raf1-RBD which brings the streptavidin-europium and anti-GST-XL665 into close proximity. Compounds which bind to KRas or stabilise the KRas:SOS complex and prevent nucleotide exchange will result in loss of the HTRF signal.

Pre-incubation		**Compounds**					**Controls**	
		10	**11**	**12**	**13**	**14**	**DMSO**	**No KRas**
A-1: KRas:GDP	Measurements	48.430, 35.594, 40.193	14.598, -7.689, -1.225	7.418, -18.160, -1.557	19.557, 12.439	51.6107, 47.1189, 44.8484	1.352, -2.447, 5.955, -4.861	99.485, 101.008, 99.508

	Mean	41.4	1.9	-4.1	16.0	47.9	0.0	100.0
	Stdev	6.5	11.5	13.0	5.0	3.4	4.7	0.9
A-2: KRas:GDP + SOS	Measurements	99.506, 102.565, 101.045	98.255, 96.861, 94.349	100.245, 98.688, 98.279	101.077, 98.247, 99.179	101.611, 100.305, 100.471	2.075, 22.415, 13.311, -18.098, -15.954, -3.749	99.533, 100.288, 100.188
	Mean	101.0	96.5	99.1	99.5	100.8	0.0	100.0
	Stdev	1.5	2.0	1.0	1.4	0.7	16.0	0.4
A-3: SOS	Measurements	2.154, -10.344, -25.342	-21.796, -18.857	-13.096	-36.586, 9.190, 17.839	19.165, 24.963, 44.560	-10.967, 7.401, 5.181, -1.615	100.291, 98.218, 101.495
	Mean	-11.2	-20.3	-13.9	-3.2	29.6	0.0	100.0
	Stdev	13.8	2.1	n/a	29.2	13.3	8.3	1.7

p Values	**Compounds**				
	10	**11**	**12**	**13**	**14**
A-1 : A-2	0.0001	0.0001	0.0002	0.0001	<0.0001
A-2 : A-3	0.0001	<0.0001	-	0.0037	0.0008
A-1 : A-3	0.0039	0.0819	-	0.4467	0.0824

Supplementary Table 2 | Inhibition of KRas:SOS functional activity by irreversible inhibitors 10-14. Inhibition of functional activity was measured following 2.5 hour pre-incubation of **10-14** with either KRas alone, a KRas:SOS mixture, or SOS alone. The mean and standard deviation of measurements are given, except for the SOS/**12** experiment where only one measurement was obtained due to a dispensing failure. p Values are shown comparing each of the three assays with one another.

MANT-dGDP nucleotide exchange assays. Reagents were diluted in 20 mM HEPES, 150 mM NaCl, 5 mM $MgCl_2$, 0.01% Tween-20. Results are given in **Supplementary Table 3**.

MANT-dGDP pre-equilibration. In three separate 400 μL reactions, KRas (1 μM), KRas(G12V) (1 μM) and KRas(G12C) (1 μM) were each incubated with SOS (2 μM) and MANT-dGDP (1.5 μM) (2'-Deoxy- 3'-O-(N'-methylanthraniloyl)guanosine-5'-O-diphosphate, Biolog Life # D084-05). The reactions were incubated for 4 hours to allow the MANT-dGDP to equilibrate with the unlabelled GDP bound to the purified KRas.

KRas inactivation. To monitor the inactivation of KRas, 6 μL of **12** (as a 400 μM solution) was added to a black 384 well plate (Greiner 748900). A portion of the equilibrated KRas:SOS:MANT-dGDP mixture (6 μL) was added to **12** (for a final compound concentration of 200 μM) and the plate was read kinetically (350 nm/450 nm ex/em) using a PHERAstar microplate reader (BMG LABTECH, Germany). Data for each individual well were double referenced to time zero (Time x – time zero fluorescence) and DMSO controls (Compound data – DMSO data at each time point).

	Time (min)	**0**	**5**	**10**	**15**	**20**	**25**	**30**	**35**	**40**
Ras WT	Mean	0	-1688	-2635	-5120	-5606	-5338	-6460	-5891	-6736
	Std. dev.	0	1016	1230	568	754	935	914	1343	599
Ras (G12V)	Mean	0	-1903	-3874	-5164	-6113	-6877	-7303	-7532	-7519
	Std. dev.	0	358	336	907	726	684	878	959	1041
Ras (G12C)	Mean	0	-3536	-4647	-6489	-7956	-8163	-8371	-9221	-8883
	Std. dev.	0	211	407	1075	724	673	174	839	86
Ras WT (xs GDP)	Mean	0	-1581	-2726	-4640	-5153	-5803	-6367	-6450	-7599
	Std. dev.	0	599	539	725	1059	853	875	1027	1353

	Time (min)	**45**	**50**	**55**	**60**	**65**	**70**	**75**	**80**	**85**
Ras WT	Mean	-6669	-6607	-7348	-6796	-8022	-7327	-8486	-9225	-8592
	Std. dev.	1505	1609	1685	679	1458	1762	1745	1972	1493
Ras (G12V)	Mean	-7800	-7502	-7806	-7477	-8715	-8711	-9593	-9742	-9994
	Std. dev.	1027	767	847	1037	1039	636	863	1079	929
Ras (G12C)	Mean	-9274	-9570	-9753	-9019	-9999	-10285	-10921	-11361	-11571
	Std. dev.	531	269	467	720	406	1176	519	231	949
Ras WT (xs GDP)	Mean	-7551	-7358	-7942	-7911	-8479	-8304	-8126	-8629	-8220
	Std. dev.	1615	1520	1820	1718	2009	1910	2119	2235	2148

	Time (min)	**80**	**85**	**90**	**95**	**100**	**105**	**110**	**115**	**120**
Ras WT	Mean	-9225	-8592	-9627	-10048	-10261	-10423	-10318	-10639	-10646
	Std. dev.	1972	1493	1879	1666	1810	2054	2128	2198	1535
Ras (G12V)	Mean	-9742	-9994	-9985	-10652	-10683	-10779	-11188	-11272	-11113
	Std. dev.	1079	929	868	503	1576	759	847	1094	904

Ras (G12C)	Mean	-11361	-11571	-12449	-11510	-12975	-12291	-13238	-13202	-13152
	Std. dev.	231	949	1141	542	1155	742	990	956	650
Ras WT (xs GDP)	Mean	-8629	-8220	-8419	-8431	-8258	-8522	-8452	-8410	-8650
	Std. dev.	2235	2148	2571	2688	2530	2535	2583	2783	2815

Supplementary Table 3 | Inhibition of SOS-mediated MANT-labelled nucleotide exchange by 12, with wild type Ras, and the Ras mutants G12C and G12V. The fourth experiment contained no **12**, and instead an excess of unlabelled GDP was added. This competes with the MANT-dGDP, acts as a control for the expected loss of fluorescence upon MANT-dGDP displacement and represents the rate of exchange of GDP under these experimental conditions.

Compound synthesis and characterisation

1, **2**, **4a**, **4b**, **8**, **9** & **10** are commercially available. Synthesis of **7** is described in reference (5). Synthesis and characterisation of novel compounds **3**, **5**, **6**, **11**, **12**, **13** and **14** is described below.

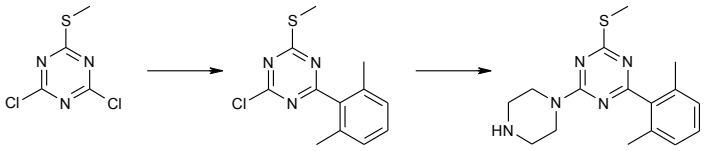

2-(2,6-Dimethylphenyl)-4-methylsulfanyl-6-piperazin-1-yl-1,3,5-triazine, 3. A 1 M solution of (2,6-dimethylphenyl)-magnesium bromide in tetrahydrofuran (5.1 mL, 5.1 mM) was added dropwise to 2,4-dichloro-6-(methylthio)-1,3,5-triazine (1.00 g, 5.1 mM) in tetrahydrofuran (2.5 mL) at 25 °C over a period of 1 minute under nitrogen. The resulting mixture was stirred at 67 °C for 18 hours. The reaction mixture was allowed to cool to room temperature and then quenched with saturated ammonium chloride (5 mL), diluted with ethyl acetate and water, shaken, and the organic layer was collected. The organic layer was then washed with saturated brine, dried over magnesium sulfate, filtered and evaporated to dryness to give crude product (1.37 g). The crude product was purified by flash silica chromatography (80 g column, Grace), with an elution gradient of 5 to 40% dichloromethane in isohexane. Pure fractions were evaporated to dryness to afford 2-chloro-4-(2,6-dimethylphenyl)-6-(methylthio)-1,3,5-triazine (0.788 g, 58.1 %) as a yellow oil which solidified on standing under high vacuum overnight. MS (*m/z*): $[MH]^+$ = 266.4; ^{1}H NMR (400 MHz, DMSO-d_6, 30 °C): δ 7.34 - 7.28 (m, 1H), 7.17 (d, *J* = 7.8 Hz, 2H), 2.60 (s, 3H), 2.16 (s, 6H).

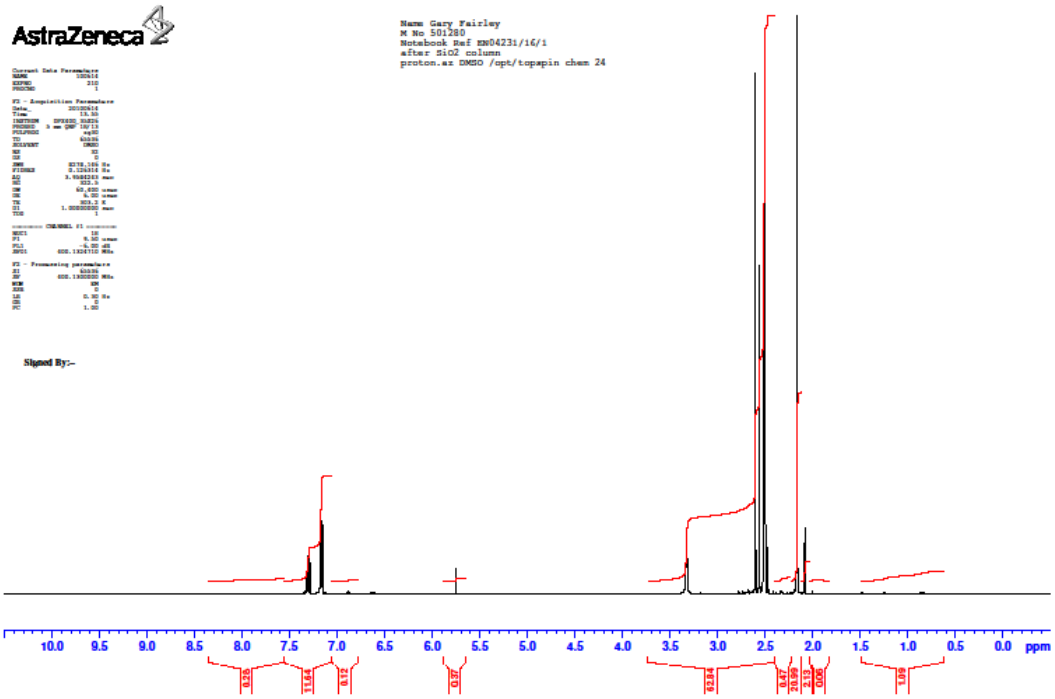

t-Butyl piperazine-1-carboxylate (0.126 g, 0.68 mM) was added in one portion to 2-chloro-4-(2,6-dimethylphenyl)-6-(methylthio)-1,3,5-triazine (0.150 g, 0.56 mM) and *N*-ethyl-*N*-isopropylpropan-2-amine (0.187 mL, 1.13 mM) in 2-pentanol (2.6 mL) at 25 °C. The resulting mixture was stirred at 100 °C for 35 minutes and allowed to cool to room temperature. The reaction mixture was evaporated to dryness, dissolved in dichloromethane (2 mL) and trifluoroacetic acid (2 mL) was added dropwise to the stirred reaction mixture at 25 °C. The reaction mixture was evaporated to dryness and the crude product was purified by ion exchange chromatography, using a 10 g SCX-2 column. The desired product was eluted from the column using a solution of ammonia in methanol (7 M) and product fractions were evaporated to dryness to afford crude product (0.163 g). The crude product was purified by preparative HPLC (Waters XBridge Prep C18 OBD column, 5µ silica, 19 mm diameter, 100 mm length), using decreasingly polar mixtures of water (containing 1% ammonia) and acetonitrile as eluents. Fractions containing the desired compound were evaporated to dryness to afford **3** (0.094 g, 52.9 %) as a colourless gum. HRMS (*m/z*): $[MH]^+$ calcd. for $C_{16}H_{21}N_5S$: 316.15904; found 316.15912; ^{1}H NMR (400 MHz, DMSO-d_6, 21 °C): δ 7.21 (dd, *J* = 8.0, 7.1 Hz, 1H), 7.09 (d, *J* = 7.5 Hz, 2H), 3.82 - 3.63 (m, 4H), 2.81 - 2.67 (m, 4H), 2.47 (s, 3H), 2.13 (s, 6H); ^{13}C NMR (126 MHz, DMSO-d_6, 30 °C): δ 180.44, 172.59, 162.11, 137.73, 134.56, 128.17, 127.39, 45.35, 44.32, 44.20, 19.44, 12.57.

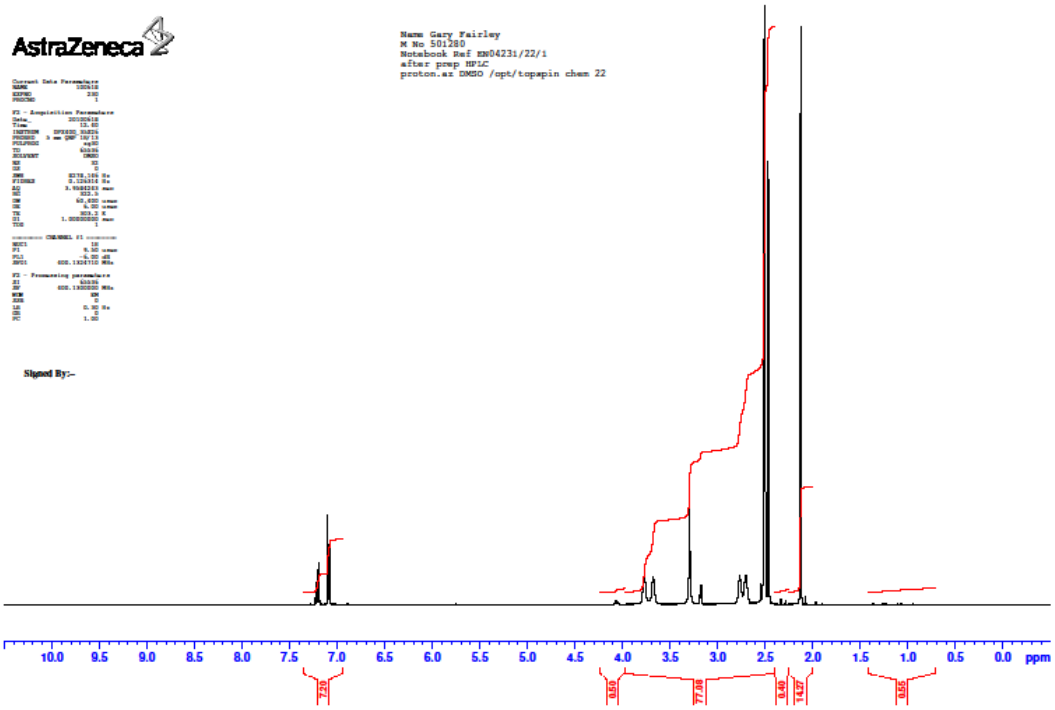

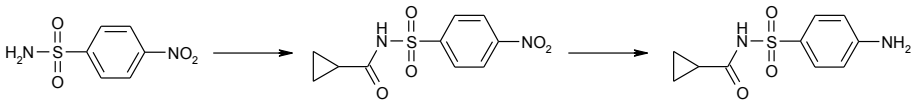

***N*-(4-Aminophenyl)sulfonylcyclopropanecarboxamide, 5.** Cyclopropanecarbonyl chloride (0.114 mL, 1.26 mM) was added to 4-nitrobenzenesulfonamide (0.254 g, 1.26 mM), triethylamine (0.437 mL, 3.14 mM) and *N*,*N*-dimethylpyridin-4-amine (0.015 g, 0.13 mM) in THF (6 mL) at room temperature under nitrogen. The resulting mixture was stirred at ambient temperature for 1 hour. The reaction mixture was diluted with water (50 mL) and washed with 2 N HCl (50 mL). The aqueous layer was removed and the organics further washed with water (50 mL), then brine (50 mL), and finally dried over magnesium sulfate and concentrated under reduced pressure onto silica. The crude product was purified by flash silica chromatography, with an elution gradient of 0 to 5 % methanol in dichloromethane. Pure fractions were evaporated to dryness to afford *N*-(4-nitrophenylsulfonyl)cyclopropanecarboxamide (0.350 g, 100 %) as a cream solid. MS (*m/z*): $[MH]^-$ = 269.35; ^{1}H NMR (400 MHz, DMSO-d_6, 21 °C): δ 12.10 - 12.00 (m, 1H), 8.43 (d, *J* = 8.9 Hz, 2H), 8.16 (d, *J* = 8.9 Hz, 2H), 1.75 - 1.66 (m, 1H), 0.85 (dq, *J* = 7.1, 3.7, 3.7, 3.4 Hz, 2H), 0.74 - 0.68 (m, 2H).

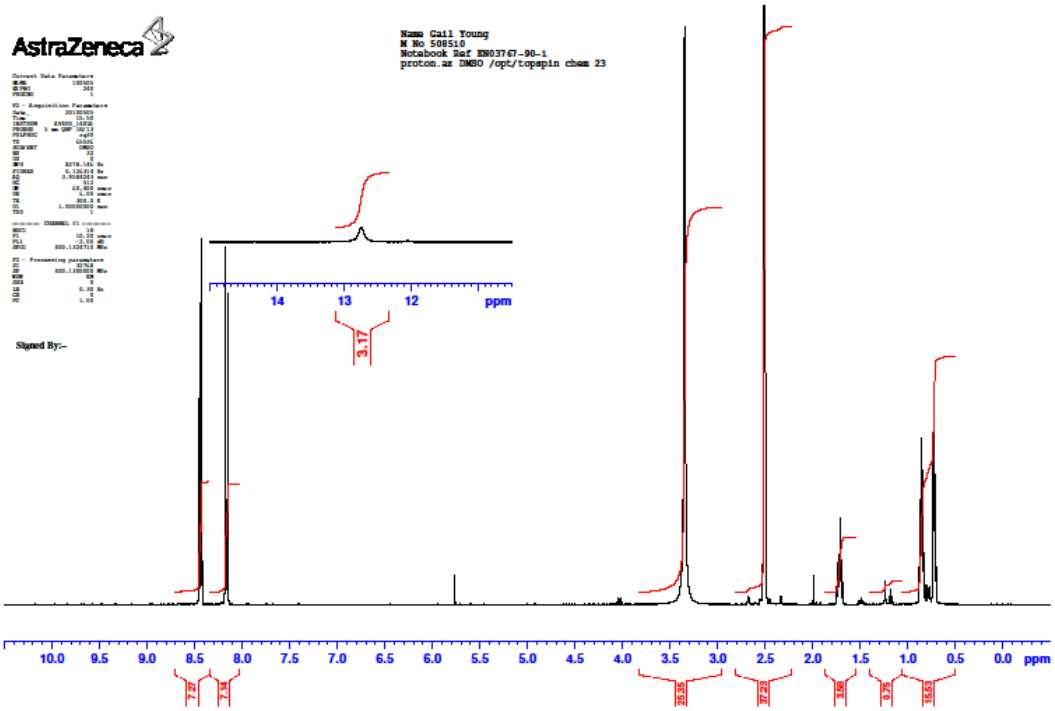

N-(4-Nitrophenylsulfonyl)cyclopropanecarboxamide (0.290 g, 1.08 mM) was added to a reactor tube and dissolved in ethyl acetate (5 mL). This tube was evacuated and purged with nitrogen three times. Palladium 10% on carbon (0.017 mg, 0.02 mM) was then added in a single portion and the flask evacuated and purged with nitrogen a further three times and with hydrogen twice. The suspension was then stirred under an atmosphere of hydrogen at 25 °C for 18 hours. The reaction mixture was filtered through celite then the crude product was purified by preparative HPLC (Waters SunFire column, 5µ silica, 19 mm diameter, 100 mm length), using decreasingly polar mixtures of water (containing 0.1% formic acid) and acetonitrile as eluents. Fractions containing the desired compound were evaporated to dryness to afford **5** (0.202 g, 78 %) as a white solid. HRMS (*m/z*): $[MH]^+$ calcd. for $C_{10}H_{12}N_2O_3S$: 241.06414; found 241.06416; ^{1}H NMR (400 MHz, DMSO-d_6, 21 °C): δ 11.83 (s, 1H), 7.52 (d, J = 8.7 Hz, 2H), 6.59 (d, J = 8.7 Hz, 2H), 6.08 (s, 2H), 1.73 - 1.58 (m, 1H), 0.80 - 0.72 (m, 2H), 0.72 - 0.64 (m, 2H); ^{13}C NMR (126 MHz, DMSO-d_6, 30 °C): δ 171.65, 153.50, 129.66, 123.84, 112.21, 13.59, 8.17.

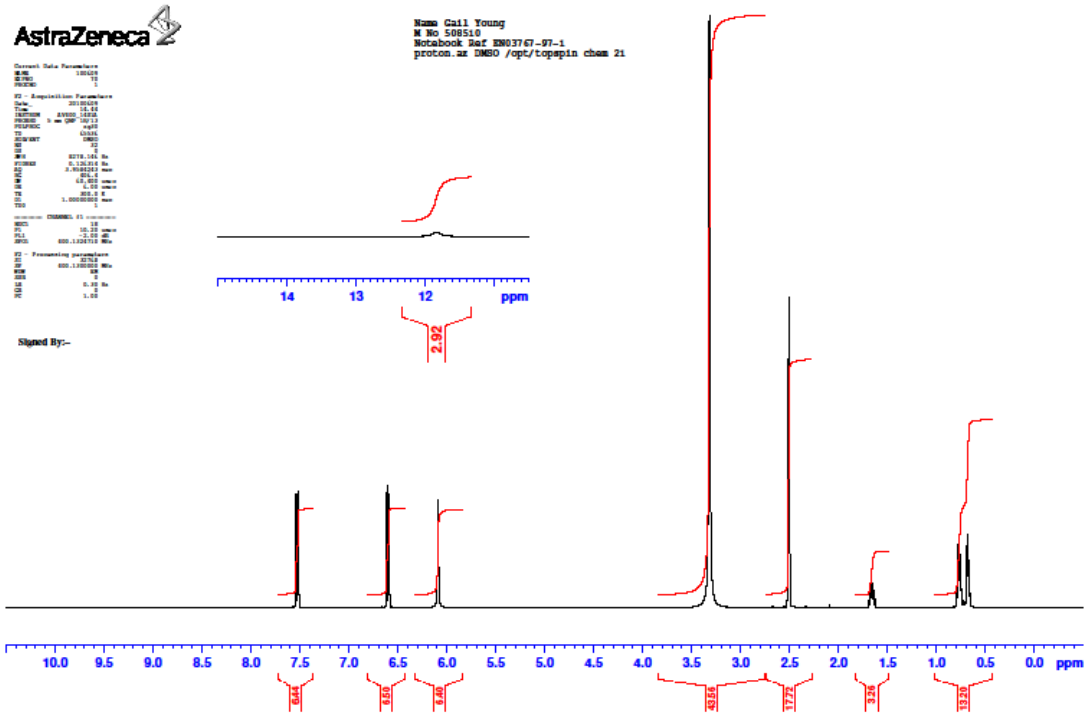

1-(4-Aminophenyl)sulfonylpiperidin-2-one, 6. A mixture of palladium 10% on carbon (0.344 g, 0.32 mM) and 1-(4-nitrophenylsulfonyl)piperidin-2-one (0.918 g, 3.23 mM) were stirred in a solution of dimethylformamide (30 mL) under an atmosphere of hydrogen at 25 °C for 24 hours. The reaction mixture was filtered, concentrated and diluted with ethyl acetate (75 mL), and washed sequentially with water (2 x 75 mL) and saturated brine (75 mL). The organic layer was dried over magnesium sulfate, filtered and evaporated to afford desired product, which was triturated with acetonitrile, filtered and evaporated to dryness to give **6** (0.610 g, 74 %). HRMS (*m/z*): $[MH]^+$ calcd. for $C_{11}H_{14}N_2O_3S$: 255.07979; found 255.07985; ^{1}H NMR (400 MHz, DMSO-d_6, 21 °C): δ 7.57 - 7.51 (m, 2H), 6.62 - 6.55 (m, 2H), 6.13 (s, 2H), 3.79 - 3.72 (m, 2H), 2.31 (t, J = 6.7 Hz, 2H), 1.79 (ddd, J = 9.6, 7.3, 4.7 Hz, 2H), 1.71 - 1.61 (m, 2H); ^{13}C NMR (126 MHz, DMSO-d_6, 30 °C): δ 169.61, 153.72, 130.31, 130.20, 123.28, 112.09, 112.00, 46.30, 33.66, 22.72, 19.71.

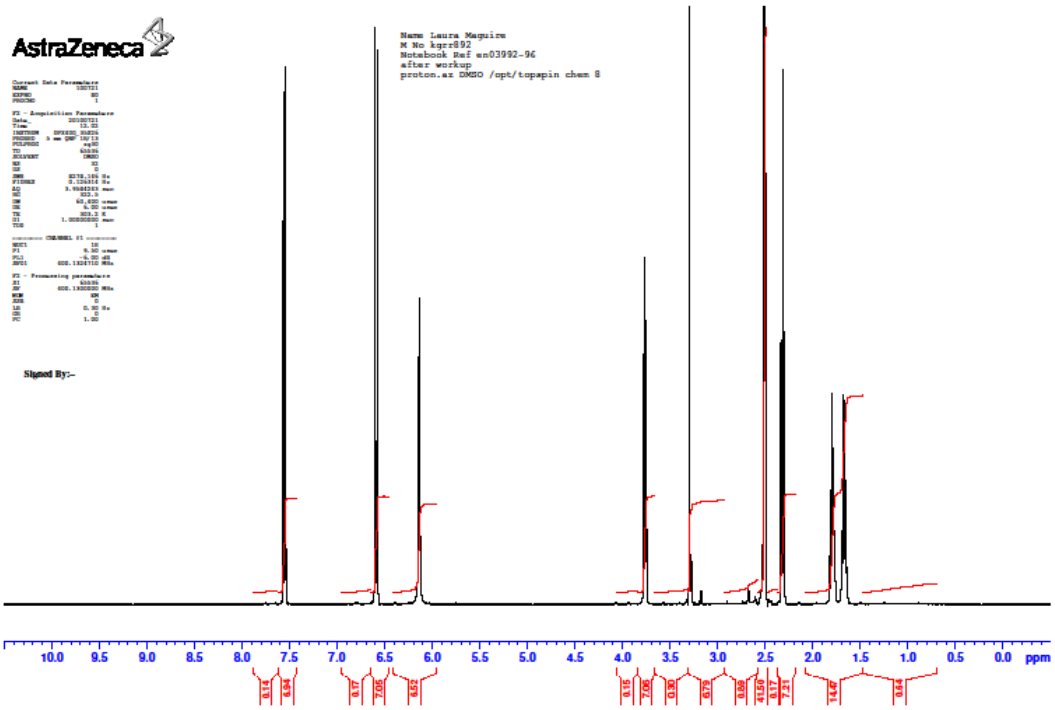

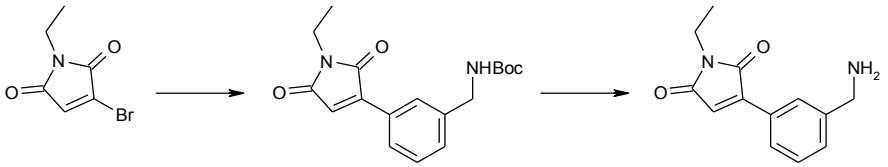

3-[3-(Aminomethyl)phenyl]-1-ethyl-pyrrole-2,5-dione, 11. 3-Bromo-1-ethyl-1H-pyrrole-2,5-dione (0.250 g, 1.23 mM) was added to 4-((*tert*-butoxycarbonylamino)-methyl)phenylboronic acid (0.308 g, 1.23 mM), $PdCl_2$(dppf) (0.067 g, 0.09 mM) and cesium fluoride (0.372 g, 2.45 mM) in dioxane (10 mL) at 20 °C. The reaction was degassed with nitrogen for 10 minutes and then heated at 70 °C for 1 hour. The reaction mixture was filtered through celite and the filtrate was concentrated *in vacuo*. The crude product was purified by flash silica chromatography with an elution gradient of 50 to 100% diethyl ether in heptane. Pure fractions were evaporated to dryness to afford *tert*-butyl 4-(1-ethyl-2,5-dioxo-2,5-dihydro-1H-pyrrol-3-yl)benzylcarbamate (0.305 g, 75 %) as a yellow gum.

tert-Butyl 3-(1-ethyl-2,5-dioxo-2,5-dihydro-1H-pyrrol-3-yl)benzylcarbamate (0.320 g, 0.97 mM) was added to 6.0 N HCl in propan-2-ol (10 mL) and the reaction was stirred for 1 hour. Diethyl ether (10 mL) was then added to the reaction and the mixture was stirred for 30 minutes to afford a solid which was collected by filtration and dried under vacuum to give **11** (0.102 g, 39.5 %) as a white solid. HRMS (*m/z*): $[MH]^+$ calcd. for $C_{13}H_{14}N_2O_2$: 231.11280 ; found 231.11285; ^{1}H NMR (400 MHz, DMSO-d_6, 21 °C): δ 8.47 (s, 2H), 8.16 (s, 1H), 8.03 (dt, *J* =

7.7, 1.3 Hz, 1H), 7.64 (d, J = 7.8 Hz, 1H), 7.56 (dd, J = 7.7, 7.7 Hz, 1H), 7.28 (s, 1H), 4.08 (s, 2H), 3.51 (q, J = 7.2 Hz, 2H), 1.14 (t, J = 7.2 Hz, 3H); ^{13}C NMR (126 MHz, DMSO-d_6, 30 °C): δ 170.2, 169.9, 142.2, 134.8, 131.2, 129.0, 129.1, 128.4, 125.5, 42.0, 32.3, 13.6.

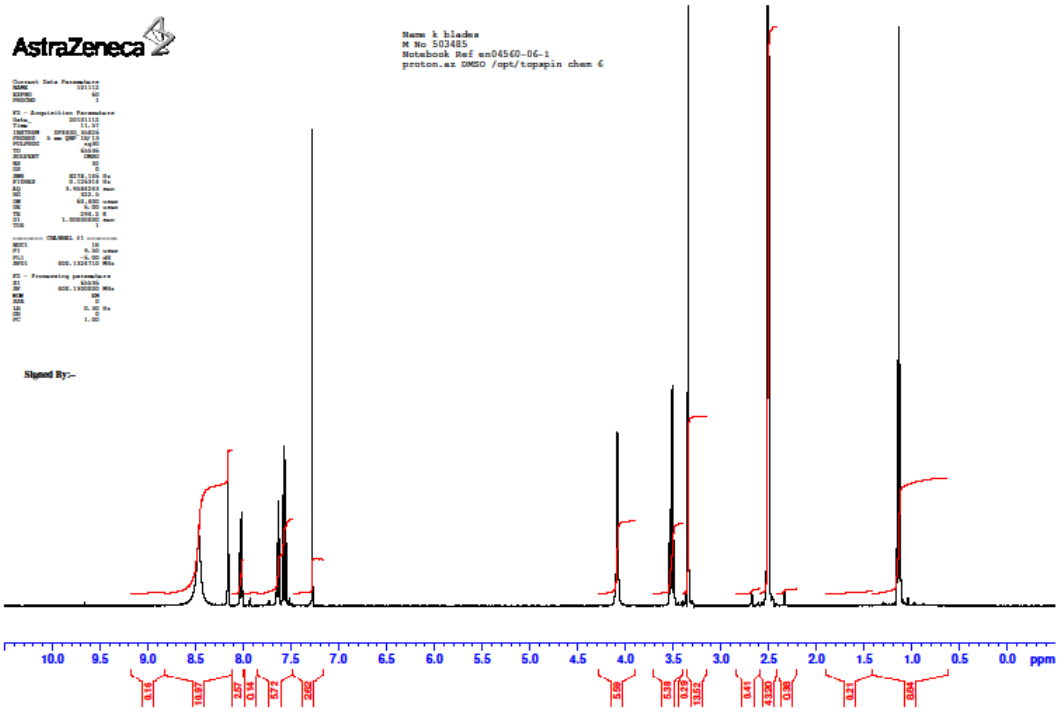

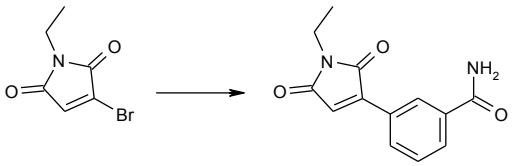

3-(1-Ethyl-2,5-dioxo-pyrrol-3-yl)benzamide, 12. 3-Bromo-1-ethyl-1H-pyrrole-2,5-dione (0.250 g, 1.23 mM) was added to 3-carbamoylphenylboronic acid (0.22 g, 1.35 mM), cesium fluoride (0.372 g, 2.45 mM) and $PdCl_2$(dppf) (0.067 g, 0.09 mM) in dioxane (10 mL)/water (1.0 mL). The reaction was heated to 70 °C for 1 hour, then quenched with water (50 mL). The resulting mixture was extracted with dichloromethane (2 x 50 mL) then the organic layers were dried over magnesium sulfate, filtered and evaporated to afford a brown solid. The crude solid was triturated with dichloromethane to give a solid which was collected by filtration and dried under vacuum to give **12** (0.150 g, 50 %) as a white solid. HRMS (*m/z*): $[MH]^+$ calcd. for $C_{13}H_{12}N_2O_3$: 231.11280; found 231.11285; ^{1}H NMR (400 MHz, DMSO-d_6, 21 °C): δ 8.46 (s, 1H), 8.14 (d, J = 7.8 Hz, 1H), 8.07 (s, 1H), 7.98 (d, J = 7.8 Hz, 1H), 7.60 (t, J = 7.8 Hz, 1H), 7.53 (s, 1H), 7.33 (s, 1H), 3.51 (q, J = 7.2 Hz, 2H), 1.14 (t, J =

7.2 Hz, 3H); ^{13}C NMR (126 MHz, DMSO-d_6, 30 °C): δ 170.2, 170.0, 167.20, 142.2, 134.9, 131.0, 129.5, 128.9, 128.8, 127.7, 125.8, 32.3, 13.6.

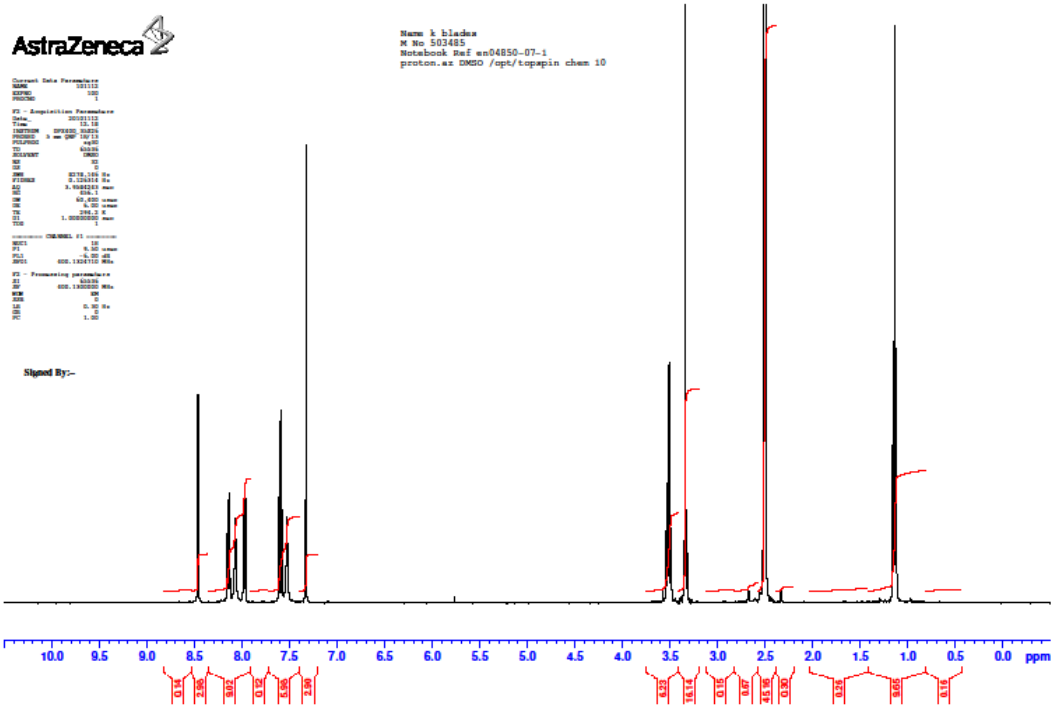

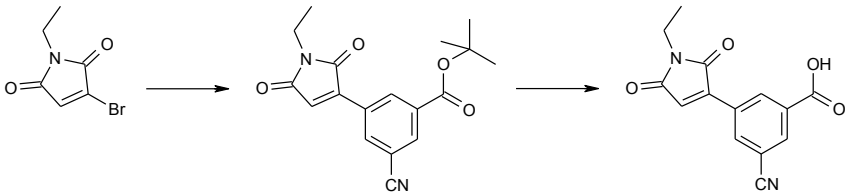

3-Cyano-5-(1-ethyl-2,5-dioxo-pyrrol-3-yl)benzoic acid, 13. *tert*-Butyl 3-cyano-5-(4,4,5,5-tetramethyl-1,3,2-dioxaborolan-2-yl)benzoate (0.538 g, 1.23 mM) was added to $PdCl_2$(dppf) (0.067 g, 0.09 mM), 3-bromo-1-ethyl-1H-pyrrole-2,5-dione (0.250 g, 1.23 mM) and cesium fluoride (0.372 g, 2.45 mM) in dioxane (15 mL) at 20 °C. The reaction was degassed with nitrogen for 10 minutes and was then heated at 70 °C for 2 hours. Water (1 mL) was added and the mixture was heated a further 2 hours at 70 °C. The reaction mixture was filtered through celite. The filtrate was concentrated and the residue redissolved in dichloromethane. The crude product was purified by flash silica chromatography with an elution gradient of 0 to 30% ethyl acetate in heptane. Pure fractions were evaporated to dryness to afford *tert*-butyl 3-cyano-5-(1-ethyl-2,5-dioxo-2,5-dihydro-*1H*-pyrrol-3-yl)benzoate (0.250 g, 63 %) as a pale yellow solid. ^{1}H NMR (400 MHz, DMSO-d_6, 21 °C): δ 8.82 (t, J = 1.6 Hz,

1H), 8.64 (t, *J* = 1.6 Hz, 1H), 8.36 (t, *J* = 1.5 Hz, 1H), 7.55 (s, 1H), 3.53 (q, *J* = 7.2 Hz, 2H), 1.59 (s, 9H), 1.15 (t, *J* = 7.2 Hz, 3H).

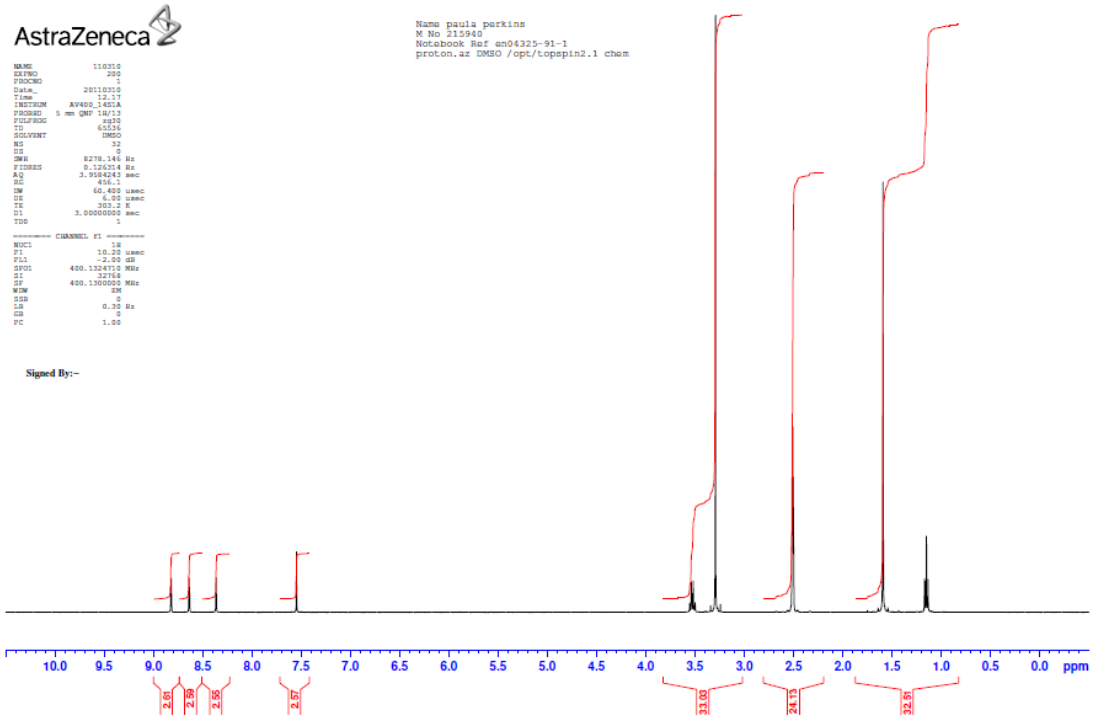

Trifluoroacetic acid (3.00 mL) was added dropwise to a solution of *tert*-butyl 3-cyano-5-(1-ethyl-2,5-dioxo-2,5-dihydro-*1H*-pyrrol-3-yl)benzoate (0.235 g, 0.72 mM) in dichloromethane (6 mL) cooled to 0 °C, then allowed to warm to ambient temperature and stirred for 1.5 hours. The reaction mixture was evaporated to dryness to afford product as an off-white solid, then triturated with diethyl ether and filtered. The resulting solid was dried under vacuum at 40 °C overnight to afford **13** (0.112 g, 58 %) as a white solid. HRMS (*m/z*): $[MH]^-$ calcd. for $C_{14}H_{10}N_2O_4$: 269.05568; found 269.05701; ^{1}H NMR (400 MHz, DMSO-d_6, 21 °C): δ 13.72 (s, 1H), 8.85 (t, *J* = 1.5 Hz, 1H), 8.64 (t, *J* = 1.5 Hz, 1H), 8.38 (t, *J* = 1.4 Hz, 1H), 7.54 (s, 1H), 3.53 (q, *J* = 7.2 Hz, 2H), 1.15 (t, 3H); ^{13}C NMR (101 MHz, DMSO-d_6, 30 °C): δ 169.78, 169.56, 165.16, 139.74, 135.70, 133.98, 133.06, 132.64, 130.57, 127.87, 117.45, 112.64, 32.43, 13.52.

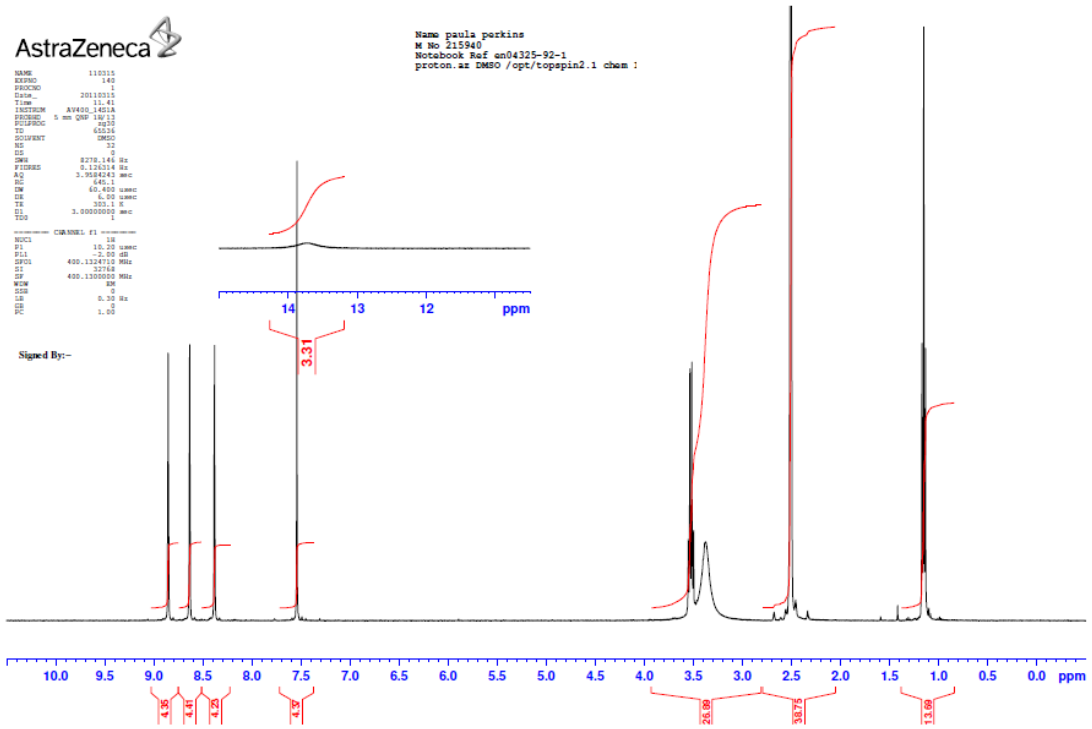

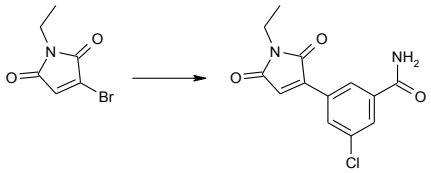

3-Chloro-5-(1-ethyl-2,5-dioxo-pyrrol-3-yl)benzamide, 14. 3-Carbamoyl-5-chlorophenylboronic acid (0.244 g, 1.23 mM) was added to $PdCl_2$(dppf) (0.067 g, 0.09 mM), 3-bromo-1-ethyl-1H-pyrrole-2,5-dione (0.250 g, 1.23 mM) and cesium fluoride (0.370 g, 2.45 mM) in dioxane (15 mL) and water (1 mL) at 20 °C. The reaction was degassed with nitrogen for 10 minutes and was then heated at 70 °C for 2 hours. The reaction mixture was filtered through celite. The filtrate was concentrated and the residue redissolved in dichloromethane. The crude product was purified by flash silica chromatography with an elution gradient of 40 to 100% ethyl acetate in heptane. Pure fractions were evaporated to dryness and then triturated with diethyl ether to afford **14** (0.104 g, 31 %) as a pale yellow solid. HRMS (*m/z*): $[MH]^-$ calcd. for $C_{13}H_{11}N_2O_3Cl$: 277.03870; found 277.03854; ^{1}H NMR (400 MHz, DMSO-d_6, 21 °C): δ 8.43 (t, *J* = 1.5 Hz, 1H), 8.21 (t, *J* = 1.7 Hz, 1H), 8.13 (s, 1H), 8.01 - 8.03 (m, 1H), 7.62 (s, 1H), 7.42 (s, 1H), 3.52 (q, *J* = 7.2 Hz, 2H), 1.15 (t, *J* = 7.2 Hz, 3H); ^{13}C NMR (101 MHz, DMSO-d_6, 30 °C): δ 169.87, 169.68, 165.78, 140.63, 136.68, 133.52, 130.82, 130.32, 128.90, 127.04, 126.39, 32.38, 13.56.

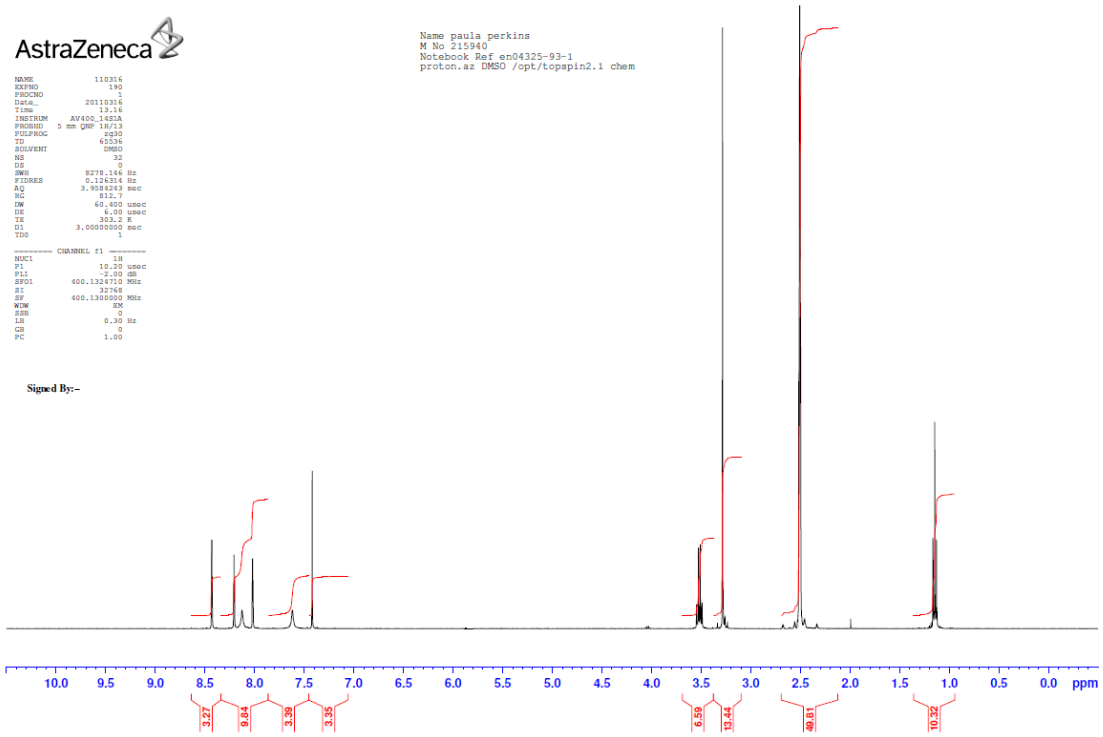

References for Supporting Information

29. Pervushin, K. V.; Wider, G.; Wüthrich, K. Single transition-to-single transition polarization transfer (ST2-PT) in [^{15}N,^{1}H]-TROSY. *J. Biomol. NMR.* **1998**, *12*, 345-348.

30. Winn, M. D.; Ballard, C. C.; Cowtan, K. D.; Dodson, E. J.; Emsley, P.; Evans, P. R.; Keegan, R. M.; Krissinel, E. B.; Leslie, A. G. W.; McCoy, A.; McNicholas, S. J.; Murshudov, G. N.; Pannu, N. S.; Potterton, E. A.; Powell, H. R.; Read, R. J.; Vagin, A.; Wilson, K. S. Overview of the CCP4 suite and current developments. *Acta. Cryst.* **2011**, *D67*, 235-242.

31. Vonrhein, C.; Flensburg, C.; Keller, P.; Sharff, A.; Smart, O.; Paciorek, W.; Womack, T.; Bricogne, G. Data processing and analysis with the autoPROC toolbox. *Acta. Cryst.* **2011**, *D67*, 293-302.

32. Smart, O. S.; Womack, T. O.; Flensburg, C.; Keller, P.; Paciorek, W.; Sharff, A.; Vonrhein, C.; Bricogne, G. Exploiting structure similarity in refinement: automated NCS and target-structure restraints in BUSTER. *Acta. Cryst.* **2010**, *D68*, 368-380.

33. Emsley, P.; Lohkamp, B.; Scott, W. G.; Cowtan, K. Features and Development of Coot. *Acta. Cryst.* **2010**, *D66*, 486-501.